Available online at www.sciencedirect.com
SCIENCE DIRECT
Journal of Asian Earth Sciences 26 (2006) 489–508
Journal of Asian Earth Sciences
www.elsevier.com/locate/jaes

Geochemistry of sedimentary rocks from mélange and flysch units south of the Yarlung Zangbo suture zone, southern Tibet

C. Dupuis[a,*], R. Hébert[a], V. Dubois-Côté[a], C. Guilmette[a], C.S. Wang[b], Z.J. Li[b]

[a]*Département de Géologie et Génie Géologique, Université Laval, Sainte-Foy, Que., Canada G1K 7P4*
[b]*Chengdu University of Technology, Chengdu, Sichuan 610059, People's Republic of China*

Received 20 October 2003; accepted 1 November 2004

Abstract

The Mesozoic Yamdrock mélange and the Triassic flysch lie immediately south of the Yarlung Zangbo Suture Zone (YZSZ) ophiolitic belt, in southern Tibet. The whole-rock chemical signature of sandstones (mostly greywackes), red shales and black shales of the Yamdrock mélange and flysch units do not present significant variations between the different rock types and geological units, and is concordant with a continental passive margin source. Despite fairly important chemical weathering, the geochemical signature was not affected by significant sedimentary recycling nor significant heavy-mineral accumulation. REE patterns show an enrichment in LREE typical of shales and indicate that the Neo-Tethyan turbidites mostly derive from a felsic old upper continental crust source. Slight enrichments in Ti and Sc indicate a mafic contribution that could originate from mafic blocks of enriched intraplate geochemical affinity found in the sedimentary units. Sedimentary rocks from both units were thus derived from the old Indian continental crust, including granitic and intraplate mafic blocks, but were deposited in different tectonic settings in the Neo-Tethys ocean. The homogeneity of the YZSZ data, which cover the whole Neo-Tethyan basin, and correlation with Himalayan data support the formation of all Himalayan lithotectonic units along a continuous passive margin of Northern India.

Keywords: Flysch; Mélange; Passive margin; Mafic blocks; Granite; Tibet

1. Introduction

The Yarlung Zangbo Suture Zone (YZSZ), in Southern Tibet, is a major tectonic feature lying between India and Asia, and marks the location where the Neo-Tethyan oceanic domains were consumed by northward subduction under the Lhasa Terrane during the Cretaceous (Tapponnier et al., 1981a; Allègre et al., 1984; see review by Searle et al., 1987). The present work is part of a Sino-Canadian project initiated in 1998 and devoted to the geodynamic reinterpretation of the central YZSZ ophiolitic massifs (Hébert et al., 2000, 2001, 2003; Huot et al., 2002; Dubois-Côté et al., 2003; Dubois-Côté, 2004), and the mélange and flysch units lying immediately south of the ophiolitic chain, i.e. the Early Cretaceous ophiolitic serpentinite mélange, the Mesozoic Yamdrock mélange and the Triassic flysch (Figs. 1 and 2). The YZSZ is one of the six main tectonic units forming the Himalayan chain, which are from north to south, the Trans-Himalayan zone (Andean-type northern margin of Tethys), the YZSZ, the Tibetan Sedimentary Series, the High Himalayan Crystalline Series, the Lesser Himalayan Series, and the sub-Himalaya comprising sediments eroded from the Himalayan orogen (e.g. Hodges, 2000; Najman et al., 2000).

Several authors have used Nd and Sr isotopic data to differentiate between the Greater Himalaya (GH), the Lesser Himalaya (LS) and the Tethyan Himalaya (TH; including the Tibetan Sedimentary Series and YZSZ sedimentary units), and to determine Tertiary Himalayan foreland basin provenance (e.g. France-Lanord et al., 1993; Galy et al., 1996; Najman et al., 2000; Huyghe et al., 2001; Robinson et al., 2001). However, the TH standard values were derived from only six samples (France-Lanord et al., 1993) and few observations have been added since. The lack of new data

* Corresponding author. Tel.: +1 418 656 2193; fax: +1 418 656 7339.
E-mail address: cedupuis@ggl.ulaval.ca (C. Dupuis).

1367-9120/$ - see front matter © 2004 Elsevier Ltd. All rights reserved.
doi:10.1016/j.jseaes.2004.11.002

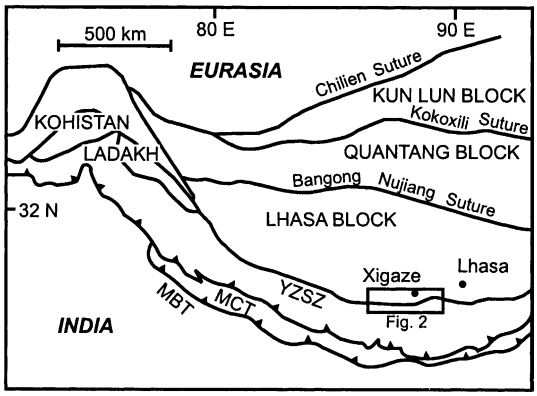

Fig. 1. Schematic tectonic map of the Himalayas, the Tibetan Plateau and surrounding areas showing the different crustal blocks separated by suture zones (modified after Huot et al., 2002). MBT: main boundary thrust, MCT: main central thrust, YZSZ: Yarlung Zangbo Suture Zone.

from the TH sequence has led to an intense debate between Myrow et al. (2003) and DeCelles et al. (2000) on whether these three Himalayan lithotectonic units can be clearly distinguished on the grounds of isotopic values and detrital zircon ages. In that sense, three models have been proposed to explain the stratigraphic differences between the three Himalayan lithotectonic zones: the 'continuous margin' model, in which the three zones represent parts of a single ancient passive margin, the 'crystalline axis' model, in which the Greater Himalaya represent a basement high separating the Lesser Himalaya depositional basin from the Tethyan Himalaya passive margin, and the 'accreted terrane' model, in which the Greater Himalaya represents the basement of an exotic terrane overlain by the Tethyan Himalaya sedimentary sequence (Myrow et al., 2003 and references therein). Although each model predicts a unique set of stratigraphic, biogeographic, and geochronologic patterns (Myrow et al., 2003), only the first two models (continuous margin and crystalline axis) would predict a common source for the three Himalayan zones based on geochemical data.

The aim of the present paper is not to define the stratigraphic characteristics of these units, a work thoroughly carried out by Liu and Einsele (1996, 1999), for example, but to fill an important gap in our geochemical knowledge of these units. As just mentioned, several isotopic studies have been conducted on rocks of the Himalayan Series, including the YZSZ, but few trace element data are available for sedimentary rocks of the same area. We present new major- and trace-element geochemical data on sandstones and shales from the Mesozoic

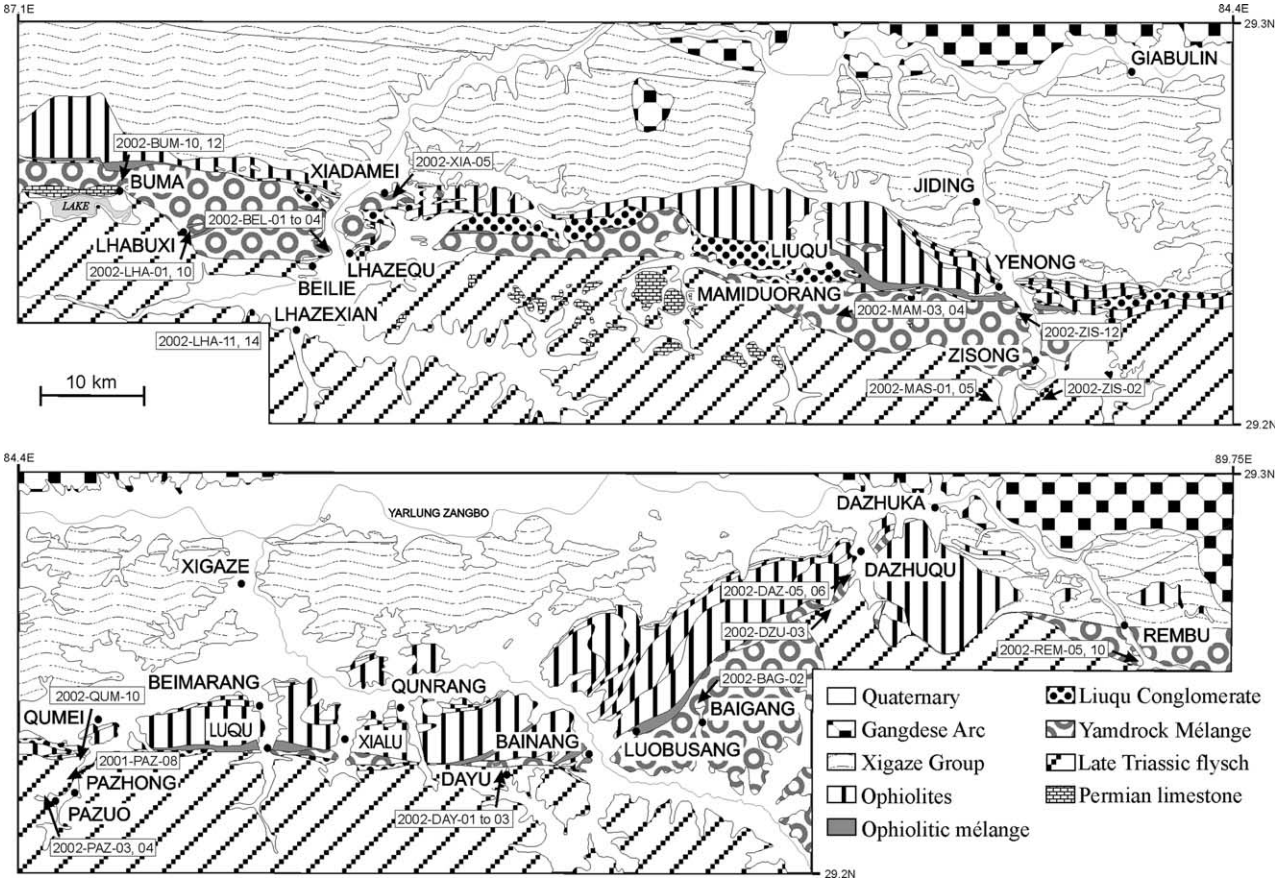

Fig. 2. Geological map of the Yarlung Zangbo Suture Zone showing the sampling regions (modified after Wang et al., 1984). The enlarged region of Jiding/Zisong shows all geological units where rocks of the present study were sampled. Locations of samples indicated by arrows and sample numbers.

Yamdrock mélange and Triassic flysch. The geochemistry of these sedimentary rocks provides information on their formation, depositional mode and provenance. It can even help constrain the geodynamic significance of alkaline mafic and granitic rocks incorporated into these sedimentary units.

2. Geological setting

India collided diachronously with Asia in Late Cretaceous to Early Tertiary time (~70–40 Ma) (e.g. Patriat and Achache, 1984; Jaeger et al., 1989; Gaetani and Garzanti, 1991; Klootwijk et al., 1992, 1994; Beck et al., 1995; Lee and Lawver, 1995; Le Fort, 1996; Rowley, 1996; Matte et al., 1997; see review by Yin and Harrison, 2000), inducing significant crustal shortening and initiating the formation of the Himalayan Mountain Belt and the uplift of the Tibetan Plateau. The Tibetan Plateau is made of several terranes, the Lhasa Terrane being the southernmost and the last to have been accreted to the growing Asian continent (Fig. 1). The southern margin of the Lhasa Terrane experienced a rifting event in the Late Triassic, which marks the initial separation of Lhasa from India and opening of the Neo-Tethys separating those two continental masses (Gaetani and Garzanti, 1991). During the Cretaceous, the Neo-Tethys gradually disappeared by northward subduction beneath the Lhasa Terrane, leading to the India–Asia collision in the Early Tertiary. At least two subduction zones were necessary to eliminate the Neo-Tethys (e.g. Aitchison et al., 2000; Wang et al., 2000; Mahéo et al., 2004). Available geochronological data (Girardeau et al., 1984; Göpel et al., 1984; Miller et al., 2003; Zyabrev et al., 1999; Ziabrev et al., 2003; Aitchison et al., 2003; Guilmette and Hébert, 2003) indicate that the intra-oceanic subduction systems, to which the YZSZ ophiolites probably belonged, was active from at least Late Jurassic to the end of the Early Cretaceous.

The Yarlung Zangbo (also called the Indus-Tsangpo) Suture Zone (YZSZ) is composed mainly of remnants of the Neo-Tethys ocean-floor and marks a major suture between the Indian Plate, to the south, and the Lhasa Terrane of Tibet, to the north. The YZSZ is thus the southernmost and the youngest of the sutures that divide the Tibetan Plateau into various E–W terranes (Fig. 1). It is characterized by a more or less continuous ophiolitic chain. The YZSZ ophiolites and subsequent sedimentary formations were first thrust (obducted) to the south onto the Indian continent, then backthrust to the north, and finally affected by strike–slip and late E–W extensional events (Gansser, 1974; Molnar and Tapponnier, 1975; Tapponnier et al., 1981a,b; Allègre et al., 1984; Burg and Chen, 1984; Mercier et al., 1984; Ratschbacher et al., 1994; Yin et al., 1994; Harrison et al., 2000; Hodges, 2000; Yin and Harrison, 2000). Along the suture, major crustal discontinuities (Mesozoic and Cenozoic thrust fault systems) delineate three main tectonic units of different geologic, deformational and metamorphic evolutions. They are, from north to south, the active paleomargin (Lhasa Terrane), the oceanic domain (components of the Neo-Tethys ocean-floor) and the passive paleomargin (components of the northern margin of the Indian Plate) (Burg et al., 1987; Hodges, 2000).

Immediately south of the ophiolitic sequences lies a distinctive mélange of complex history. It was first described as 'wildflysch with exotic blocks' by Tapponnier et al. (1981a) and interpreted as a sedimentary mélange (Shackleton, 1981). It contains units previously referred to as infra-ophiolitic thrust sheets of radiolarites (Burg and Chen, 1984) or Upper Jurassic to Lower Cretaceous red radiolarites (Girardeau et al., 1984). It was later described as the Yamdrock mélange and interpreted as a tectonic mélange (Searle et al., 1987). Recently, Aitchison et al. (2000) renamed this unit the 'Bainang Terrane' (see also Zyabrev et al., 2000; Ziabrev et al., 2000, 2001, 2004). However, the extension, geochronological, tectonic, metamorphic and geochemical characteristics of this terrane, as well as the other compartmentalized and renamed terranes along the YZSZ, are poorly constrained, precluding use at this moment of the proposed nomenclature. Since the term 'wildflysch' is considered obsolete, we adhere to the term used by Searle et al. (1987) for this unit, i.e. the Yamdrock mélange.

This mélange consists of an imbricate thrust zone containing numerous south-verging thrust slices, which preserve an ocean floor stratigraphy (Aitchison et al., 2000). Tectonic slices of red siliceous shale and radiolarian chert, and locally alkaline basalt, dominate the northern portion of this mélange (Chang, 1984; Searle et al., 1987). To the south, the quantity of chert decreases and the unit is characterized by fine-grained, thinly bedded, deep marine shales. Deformed exotic blocks, of decimeter to kilometer size, are of different facies and ages (Mercier et al., 1984; Lin, 1984; Searle et al., 1987). Permian to Cretaceous limestones, red or green Campanian–Maestrichtian micrites, Mid-Jurassic to Early Cretaceous red, green or grey cherts (Aptian: Wu, 1993; Matsuoka et al., 2001, 2002), and blocks composed of a primary association of pillow lavas. Structural and tectonostratigraphic features of the mélange are reminiscent of a remote intra-oceanic subduction complex (Mercier et al., 1984; Searle et al., 1987; Aitchison et al., 2000), and the unit has been interpreted as consisting mostly of material off-scraped from the down-going Tethyan slab (Chang, 1984; Ziabrev et al., 2001). The matrix is composed mainly of layered pelitic rocks, containing Senonian *Globotruncana* fossils, indicating an age of at least Late Cretaceous for the mélange (Chang, 1984; Mercier et al., 1984). Detailed radiolarian stratigraphy further indicates that accretion occurred from late Aptian to at least Campanian (Zyabrev et al., 2000; Ziabrev et al., 2000, 2001), while the youngest fossils found in exotic blocks and in the matrix are Maestrichtian to

Paleocene, extending the age of the formation of this unit into the Early Tertiary (Burg and Chen, 1984).

Sediments of the Indian passive margin (Permian to Cretaceous in age) were thrust southward toward the Indian foreland during the Early Paleocene and are now represented by three major imbricated allochthonous tectonic units (Burg and Chen, 1984; Burg et al., 1987; Liu and Einsele, 1996, 1999). From north to south, the three units consist of turbidites (continental margin), carbonate flysch (northern Tethyan sediments) and a platform sequence (southern Tethyan sediments). The assemblage lies in fault contact over the Main Central Crystalline Sheet and represents deposits of progressively deeper water, up to the flysch of the YZSZ to the north. The flysch is intercalated locally with calcareous rocks and mafic to intermediate volcanic rocks, probably associated with intracontinental rifting and the formation of a continental passive margin (Chang, 1984; Dupuis et al., 2003, 2004), such as the continental tholeiitic and mildly alkaline flood basalts of the Panjal Traps of northwest India along the northern margin of the Indian Plate (Searle et al., 1987).

Tectonic conditions resulting in the formation of the flysch were encountered in the Triassic (Gansser, 1980; Gaetani and Garzanti, 1991). Moreover, the Triassic flysch sequence south of the YZSZ contains fossils (*Daonella* sp., *Halobia* sp.) of Middle Triassic to Early Jurassic age (Mercier et al., 1984). It reaches several kilometers in thickness and is structurally complex. The sequence is highly folded, verges to the south, and is affected by regional metamorphism ranging from the greenschist to the amphibolite facies (Chang, 1984; Burg et al., 1987). No mineral associations characteristic of high pressure were found. The central section (corresponding to the study area of Fig. 1) probably represents the least deformed section of Indian passive continental margin rocks anywhere in the Himalayan Belt (Searle et al., 1987). The deformation increases to the north, as the Triassic flysch is transformed from a sedimentary to a tectonic mélange, i.e. the Yamdrock mélange. The metamorphism, observed throughout the whole suture, contrasts with the normally non-metamorphic platform-type sedimentary sequence located to the south. The contact between the two units is marked by a tectonized zone, along which numerous small Early Ordovician granitic intrusions are found (Chang, 1984; Liu and Einsele, 1996).

3. Field observations

At first sight, the Yamdrock mélange and the Triassic flysch appear similar. They consist principally of flysch sequences of pelagic shales with siliciclastic turbidites. The Triassic flysch is dominated by black shales interbedded with sandstone/siltstone and local limestone (Fig. 3A). Sandstone and limestone beds, locally boudinaged, are generally centimeter to decimeter thick (Fig. 3B), although meter-thick sequences of beach-like pure sandstones were observed locally. Intercalated grey chert is scarce. Black shales are graphitic, locally containing up to 5% of oxidized pyrite crystals, usually adjacent to limestones. Late quartz veins, millimeter to centimeter wide, are frequent. By contrast, the Yamdrock mélange is more heterogeneous. In addition to interbedded black shales and sandstones, this unit is composed of widespread sequences of red and tuffaceous green shales, as well as green and red radiolarian cherts. Red and green shales and cherts are generally thinly interstratified. Blocks of sandstone, limestone, basalt and chert, of all sizes, are commonly found within or between mudstone sequences. In that case, the unit displays a block-in-matrix aspect (Fig. 3C) characteristic of a sedimentary mélange (olistostrome; Pini, 1999). However, it also locally displays some structural order by parallel orientation of blocks and matrix features and boudinage, which is more characteristic of a tectonic mélange (tectonosome; Pini, 1999). Both sedimentary units have been affected by greenschist metamorphism, grading from shales to slates to sericite schists. They are highly tectonized, having recorded the four deformation stages mentioned earlier (Fig. 3A, B, D). Exotic blocks and nappes of Permian limestones (to marbles) are found within the predominantly siliciclastic units (Fig. 2).

Mafic rocks were found in the Yamdrock mélange and in the Triassic flysch, either within mappable mafic zones (Fig. 3E) or as meter-size blocks (Fig. 3F) within the sedimentary matrix. A granitic block (about 10 m wide) was also found within the Triassic flysch. It probably corresponds to a remnant of Cambrian-early Ordovician granites generated by subduction dipping beneath northern Gondwana, including both the future Indian continental lithosphere and the Lhasa Terrane, during latest Proterozoic and earliest Paleozoic time (Yin and Harrison, 2000). Mafic rocks from the Yamdrock mélange have alkaline intraplate geochemical signatures (Dupuis et al., 2003a,b, 2004) and are interpreted as remnants of intra-oceanic seamounts (e.g. Mercier et al., 1984; Searle et al., 1987; Liu and Einsele, 1999; Aitchison et al., 2000). Mafic rocks from the flysch are interpreted to have been derived from an enriched intraplate mantle source, with additional crustal assimilation resulting from disaggregation of the Indian Plate during the opening of the Neo-Tethys ocean (Dupuis et al., 2003a,b, 2004). AFC modelling strongly suggests a felsic component analogous to Cambro-Ordovician granites as the major contaminant.

The samples from each lithological type which were analysed in this study and the locations at which they were collected are shown in Table 1.

4. Petrographic description of sandstones

On a petrographic basis, sandstones correspond to wackes with 45–55 wt% of argillaceous matrix, around 20 wt% of feldspar altered to clay, 5–25 wt% quartz,

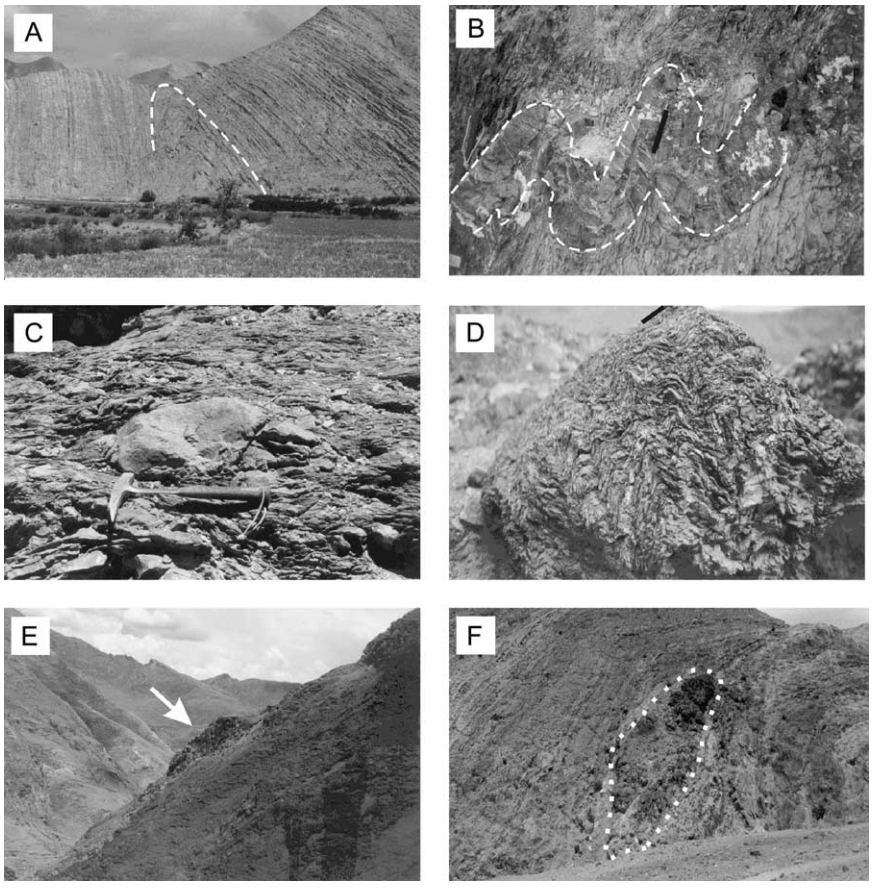

Fig. 3. Field photographs of the sedimentary units. (A) Outlined first-order fold in the Triassic flysch, Pazuo; (B) Outlined second-order folded sandstone bed in the Triassic flysch, Pazuo region (redrawn black pen shown for scale); (C) Block-in-matrix aspect in the Yamdrock mélange, Lhabuxi area (hammer shown for scale); (D) Third-order chevron folds in red cherts of the Yamdrock mélange, Lhabuxi area (redrawn black pen shown for scale); (E) Kilometer-size mafic zone within the Yamdrock mélange, Baigang area, as indicated by the white arrow; (D) Outlined meter-size mafic block within the flysch, Pazuo region.

generally less than 5 wt% of diagenetic calcite, and some chlorite, mica, opaque minerals and rock fragments (Fig. 4A). An individual sample contains abundant quartz (45 wt.%) and some altered feldspar grains (Fig. 4B). Sandstones are generally non-metamorphic, but affected by late hydrothermal circulation. Samples in which the primary minerals had been substantially replaced by calcite were not considered in this study. Red shales, usually associated with cherts, contain abundant siliceous fragments, which were selectively removed before geochemical analysis.

5. Whole-rock chemistry

5.1. Analytical methods

Whole-rock data for sandstone and shale (Tables 2a and 2b) have been analyzed by alkaline melting ICP-AES for major and trace elements and ICP-MS (VG Turbo Plasma Quad^{2+} for rare earth elements (Laboratoire INRS-ETE, Sainte-Foy, Canada). Sample dissolution was accomplished by flux fusions (Claisse fluxor). For major elements, the device accuracy is better than $\pm 5\%$, although the acceptable analytical precision is set to better than $\pm 2.5\%$. Compositions used in the graphs have been normalized on an anhydrous basis. The calculated Fe_2O_3 is assumed to represent 10% total iron analyzed as Fe_2O_3. Analytical precision is better than $\pm 1\%$ for La, Ce, Pr, Nd, Eu, Tb, Lu and Ba, $\pm 2\%$ for Sm, Gd, Dy, Ho, Er, Tm, Yb, Th, Zr, Rb and Sr, $\pm 4\%$ for Cs, Y and U, and $\pm 10\%$ for Nb. Data for USGS basalt and andesite standards analyzed with the same method at the same laboratory are reported in La Flèche et al. (1998).

5.2. Sandstones vs. shales: a compositional test

The geochemical behavior of nearby sandstones and shales, in the Beilie and Dazhuqu regions, has been compared by using chondrite-normalized REE diagrams (Fig. 5). The shales are more REE-enriched, especially in the LREE, than the sandstones. These slight differences are attributable to their different clay content. The shales are richer in incompatible elements, especially the most incompatible LREE, which are strongly partitioned in,

Table 1
Nomenclature and sample location of analysed sedimentary rocks

	Sandstone	Red shale	Black shale
Yamdrock Mélange			
Buma		2002-BUM-10	2002-BUM-12
Lhabuxi	2002-LHA-01		2002-LHA-10
Beilie	2002-BEL-02, 03		2002-BEL-01, 04
Xiadamei		2002-XIA-05	
Mamiduorang		2002-MAM-04	2002-MAM-03[a]
Zisong		2002-ZIS-12	
Qumei			2002-QUM-10[a]
Baigang		2002-BAG-02	
Dazhuqu	2002-DAZ-06		2002-DAZ-05
Rembu	2002-REM-05		2002-REM-10
No. of analyses	5	5	8
Triassic Flysch			
Lhazexian			2002-LHA-11, 14[b]
Zisong			2002-MAS-01, 05
			2002-ZIS-02
Pazuo/Pazhong			2002-PAZ-03, 04, 08
Dayu			2002-DAY-01, 02, 03[a]
Dazhuqu			2002-DZU-03
No. of analyses			13

[a] Sericite schist.
[b] Duplicated to test the precision of geochemical analyses.

or absorbed on, clay minerals (e.g. Nesbitt and Young, 1989). Nevertheless, the similar overall distribution of trace elements in the sandstones and shales allows us to plot them together on discrimination diagrams. Moreover, black shales from the Yamdrock mélange and Triassic flysch are chemically undistinguishable and will be treated as a whole in the following discussion.

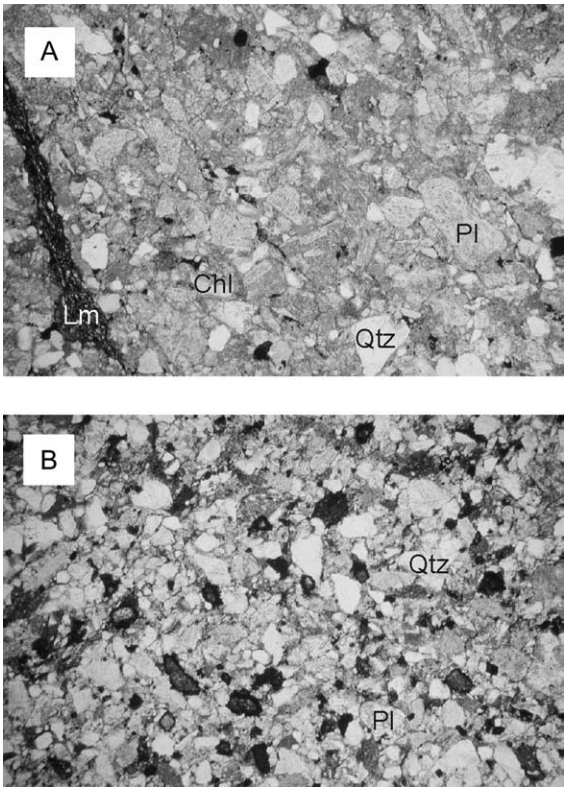

Fig. 4. Microphotographs of YZSZ sandstones. (A) Greywacke; (B) Lithic wacke. Chl, chlorite; Lm, limonite; Pl, plagioclase; Qtz, quartz.

5.3. Major elements

On the $(Fe_2O_3^T + MgO)$–Na_2O–K_2O triangular diagram of Blatt et al. (1980), four sandstones classify as sodic, whereas the quartz-rich sandstone classifies as ferromagnesian potassic (Fig. 6A). On the $\log(Na_2O/K_2O)$–$\log(SiO_2/Al_2O_3)$ diagram of Pettijohn et al. (1973), the same rocks classify as greywackes ($K_2O/Na_2O < 1$) and lithic wacke ($K_2O/Na_2O = 1$), respectively (Fig. 6B). The shales, both red and black, almost all classify as ferromagnesian potassic on the $(Fe_2O_2^T + MgO)$–Na_2O–K_2O triangular diagram. One black shale classifies as potassic. However, this shale is one of the most siliceous (SiO_2: 80.3 wt%), and other major elements, especially ferromagnesian elements, are correspondingly diluted. The shale composition is thus more representative of a relative depletion in ferromagnesian rather than an enrichment in potassium. Shales have $K_2O/Na_2O > 1$. The less siliceous rocks have SiO_2 lower than 60 wt% and Al_2O_3 slightly higher than 24 wt%, whereas the more siliceous have SiO_2 as high as 86 wt% and Al_2O_3 as low as 6.6 wt%, expressing quartz/clays feldspar ratio. SiO_2/Al_2O_3 ratios range from 2.4 to 13.

Most major elements are negatively correlated with SiO_2, reflecting the quartz dilution effect. For the sandstones, SiO_2 strongly correlates with Al_2O_3, MgO, TiO_2 and Na_2O (r of -0.97 to -0.95 at a significance level α of 0.5 and 1%, respectively), and correlates well with P_2O_5, MnO and Fe_2O_3 (r of -0.81 to -0.72 at α of 5–10%) (Table 3). The absence of significant covariation for CaO ($r = +0.26$ at $\alpha \gg 10\%$) and K_2O ($r = +0.62$ at $\alpha > 10\%$) may be explained by the mobility of these elements during weathering, diagenesis and regional metamorphism. Correlations are generally much weaker for the shales (r ranging from -0.85 to -0.13; Table 4). Nevertheless, at $\alpha = 0.1\%$, Al_2O_3 ($r = -0.85$), K_2O ($r = -0.65$) and Fe_2O_3 ($r = -0.65$) show good negative correlations with SiO_2.

5.4. Trace elements

REE patterns are LREE-enriched: La abundances vary from 7 to 35 and from 60 to 256 times chondrite for the sandstones and shales, respectively. In the same way Yb abundances vary from 4 to 12 and from 54 to 86 times chondrite, respectively (Fig. 7). An individual shale has a lower La abundance of 32 times chondrite, but a 'normal' Yb abundance of 14 times chondrite, resulting in a 'U-shaped' pattern. All rocks show a significant negative Eu anomaly. When normalized to the Post-Archean average Australian shale (PAAS, Taylor and McLennan, 1985), REE patterns are generally flat (Fig. 8). La abundances vary from 0.3 to 0.5 times PASS and from 0.4 to 1.5 times PASS for the sandstones and shales, respectively. The same way Yb

Table 2a
Compositions of sedimentary rocks of the Yamdrock mélange recalculated volatile-free

	Sandstone						Red shale				
	LHA-01	BEL-02	BEL-03	DAZ-06	REM-01	REM-05	BUM-10	XIA-05	MAM-04	ZIS-12	BAG-02
SiO_2	80.86	60.99	61.53	63.81	21.15	74.05	71.40	74.10	77.36	85.92	78.68
TiO_2	0.30	0.71	0.72	0.80	0.49	0.43	0.64	0.77	1.25	0.49	0.52
Al_2O_3	6.66	16.67	17.14	15.59	4.24	11.29	13.88	10.95	7.44	6.60	9.08
Fe_2O_3	2.88	7.02	6.99	7.71	3.00	7.04	6.01	7.06	8.05	3.86	5.21
MnO	0.05	0.09	0.08	0.11	0.06	0.04	0.13	0.16	0.19	0.14	0.03
MgO	0.79	3.20	3.29	3.52	0.84	1.22	2.14	1.75	2.64	0.84	1.72
CaO	6.01	4.05	2.95	2.18	68.28	1.25	0.63	0.56	0.63	0.17	0.57
Na_2O	1.13	6.77	6.58	5.25	0.67	4.04	2.04	0.45	0.84	0.48	0.04
K_2O	1.19	0.23	0.47	0.77	0.81	0.39	2.97	3.85	1.49	1.42	3.96
P_2O_5	0.08	0.17	0.17	0.17	0.19	0.16	0.09	0.26	0.05	0.04	0.12
LOI	5.75	5.11	4.46	4.28	35.32	2.43	3.14	3.51	3.51	2.17	2.53
Total	97.70	99.09	98.40	98.99	100.56	97.69	99.25	98.24	99.97	98.24	99.34
Cr	37.60	85.90	85.60	34.20	<10.8	105.20	66.50	55.00	44.20	27.10	49.40
Sc	4.84	15.98	15.65	17.05	4.81	5.00	11.57	14.08	13.10	8.53	11.50
Sr	107.20	201.30	174.30	157.10	1538.30	37.90	57.70	22.80	14.20	21.00	15.20
V	33.10	145.40	144.00	171.90	49.40	89.60	87.40	124.90	112.30	50.80	59.80
Rb	61.25	9.02	21.93	35.32	12.25	12.73	135.95	117.75	40.94	55.19	110.29
Y	15.56	17.04	15.75	19.71	13.73	7.47	24.83	24.93	17.89	11.63	23.15
Zr	139.08	96.59	117.70	145.04	62.79	77.04	157.68	113.39	119.10	93.54	111.53
Nb	5.70	3.90	5.03	5.51	9.79	3.61	11.65	14.25	17.23	11.45	16.35
Cs	3.62	0.57	1.16	2.70	0.50	0.70	7.87	4.15	1.42	1.28	2.19
La	18.43	12.89	14.25	15.37	9.43	20.41	35.51	32.90	14.21	14.15	30.04
Ce	35.42	27.66	30.67	34.09	21.58	31.97	73.53	95.39	35.09	39.32	80.27
Pr	4.05	3.54	3.85	4.12	2.87	3.40	8.54	8.31	3.58	3.55	7.22
Nd	14.70	14.54	15.42	16.74	12.63	12.27	31.54	32.73	14.52	13.10	27.31
Sm	2.84	3.17	3.27	3.51	2.90	2.34	5.87	6.86	3.29	2.49	5.04
Eu	0.60	0.83	0.90	0.89	0.67	0.57	1.20	1.45	0.97	0.58	1.03
Gd	2.68	3.02	2.95	3.37	2.77	2.06	5.08	6.22	3.24	2.21	4.70
Tb	0.41	0.47	0.42	0.52	0.41	0.26	0.76	0.86	0.50	0.32	0.70
Dy	2.38	2.67	2.33	3.05	2.31	1.30	4.24	4.53	2.90	1.83	3.79
Ho	0.53	0.62	0.54	0.71	0.50	0.27	0.94	1.01	0.64	0.43	0.84
Er	1.44	1.70	1.49	1.92	1.23	0.70	2.58	2.71	1.75	1.16	2.18
Tm	0.22	0.25	0.23	0.29	0.18	0.10	0.39	0.41	0.25	0.18	0.33
Yb	1.51	1.75	1.61	1.97	1.10	0.70	2.68	2.72	1.67	1.23	2.17
Lu	0.22	0.26	0.24	0.30	0.17	0.11	0.39	0.40	0.24	0.18	0.32
Hf	3.52	2.49	2.89	3.43	1.41	1.91	4.28	2.73	2.76	2.17	2.78
Ta	0.53	0.29	0.34	0.39	0.60	0.21	1.02	1.04	1.23	0.82	1.00
Th	8.29	4.85	5.77	4.30	1.08	2.90	14.41	9.26	3.58	4.90	8.51
U	1.63	1.36	1.48	1.02	0.25	0.82	2.48	1.04	0.50	0.67	1.24

	Black shale							
	BUM-12	LHA-10	BEL-01	BEL-04	MAM-03	QUM-10	DAZ-05	REM-10
SiO_2	62.07	63.66	84.32	59.75	69.29	61.82	65.38	80.26
TiO_2	0.68	0.79	0.51	0.90	1.10	1.06	0.62	0.49
Al_2O_3	13.87	18.00	10.09	22.78	14.58	17.20	19.03	9.81
Fe_2O_3	6.87	5.28	1.71	8.39	7.70	13.48	5.32	3.24
MnO	0.26	0.09	0.00	0.05	0.20	0.12	0.04	0.02
MgO	2.90	2.14	0.51	2.34	2.46	1.97	2.03	1.58
CaO	9.18	4.28	0.16	0.32	0.29	0.35	0.56	0.63
Na_2O	0.95	0.24	0.50	0.96	0.12	0.47	3.05	1.24
K_2O	2.82	4.84	2.04	4.26	4.00	3.17	3.79	2.55
P_2O_5	0.13	0.17	0.06	0.08	0.07	0.19	0.08	0.10
LOI	13.62	9.79	2.48	5.63	4.22	4.28	6.10	2.43
Total	100.68	99.18	97.67	98.71	99.18	99.26	98.62	97.32
Cr	66.40	81.60	49.80	122.40	83.30	106.20	43.80	56.90
Sc	13.51	14.09	9.42	20.99	19.41	19.52	13.48	7.30
Sr	157.00	107.30	248.50	121.10	15.20	81.90	36.70	29.70
V	100.30	114.40	66.30	164.90	161.60	154.50	99.40	55.30
Rb	118.77	211.87	115.04	240.00	161.03	176.87	175.89	122.26

(*continued on next page*)

Table 2a (*continued*)

	Black shale							
	BUM-12	LHA-10	BEL-01	BEL-04	MAM-03	QUM-10	DAZ-05	REM-10
Y	28.89	30.73	9.64	45.69	31.50	36.72	19.52	23.90
Zr	141.27	178.48	104.45	174.42	185.61	198.27	147.07	216.07
Nb	13.64	14.02	14.08	23.79	23.14	24.39	12.15	10.04
Cs	9.33	13.34	6.26	12.82	7.98	5.15	13.08	6.15
La	30.14	42.77	27.18	59.82	39.03	45.90	7.58	28.47
Ce	66.84	91.40	81.03	136.29	106.15	130.49	14.33	57.62
Pr	7.30	10.19	6.49	14.48	9.59	10.67	1.81	6.71
Nd	28.07	38.08	23.30	54.27	36.34	39.51	7.08	24.52
Sm	5.65	7.15	3.21	8.98	6.74	7.61	1.64	4.58
Eu	1.12	1.36	0.39	1.56	1.41	1.65	0.34	0.81
Gd	5.19	6.27	2.05	7.51	5.92	7.08	1.92	4.04
Tb	0.77	0.95	0.24	1.12	0.85	1.00	0.33	0.61
Dy	4.13	5.26	1.27	6.60	4.77	5.58	2.12	3.58
Ho	0.94	1.18	0.32	1.54	1.09	1.26	0.57	0.83
Er	2.44	3.16	1.01	4.11	2.99	3.33	1.86	2.25
Tm	0.34	0.47	0.18	0.58	0.43	0.47	0.31	0.34
Yb	2.30	3.12	1.29	3.86	2.88	3.30	2.39	2.33
Lu	0.34	0.46	0.20	0.56	0.42	0.48	0.39	0.32
Hf	3.10	4.86	2.34	4.04	4.16	4.69	3.43	5.35
Ta	0.87	1.28	0.91	1.48	1.47	1.64	1.06	0.87
Th	10.86	19.54	10.27	22.11	11.72	18.20	12.59	11.70
U	1.88	3.31	1.28	2.41	1.82	1.39	2.77	2.13

abundances vary from 0.25 to 0.7 and from 0.4 to 1.4, respectively. The individual shale is LREE-depleted ($(La/Yb)_N$ of 0.2). Similarly, on multi-element patterns normalized to the average upper continental crust, the only deviations from the average trend are represented by slight positive Ti anomalies (especially on patterns of sandstones), and slight negative Zr–Hf anomalies on the patterns of shales.

There is moderate but significant correlation between LREE, HREE and Al_2O_3 ($r Al_2O_3$–La = +0.62 and $r Al_2O_3$–Yb = +0.61 at $\alpha = 0.1\%$), as REE are preferentially incorporated into clay minerals. There are moderate to strong positive correlations (α of 0.1%) between the mobile elements Ba, Rb, and Th, and Al_2O_3 ($r Al_2O_3$–Rb = +0.66; $r Al_2O_3$–Th = +0.73) and K_2O ($r K_2O$–Ba = +0.65; $r K_2O$–Rb = +0.89; $r K_2O$–Th = +0.74), as these elements are also preferentially incorporated into clay minerals. Not surprisingly, correlation between Al_2O_3 and Rb–Th is much stronger for the shale population alone ($r Al_2O_3$–Rb = $r Al_2O_3$–Th = +0.91 at $\alpha = 0.1\%$). On the other hand, there is no correlation between Rb and Sr (rRb–Sr = +0.07); this is expected for detrital material derived from source rocks having undergone chemical weathering (Nesbitt and Young, 1989) due to the different behavior of Rb and Sr during weathering processes. Rb/Sr ratios range from 0.3 to 10.6 for the shales, and from 0.05 to 0.6 for the sandstones. The strong positive correlations between Th and LREE (rLa–Th = +0.89 at $\alpha = 0.1\%$) further suggests that Th was partitioned among the felsic detrital material. As a consequence, Th/U ratios are very fractionated in the shales (average of 7.7 ± 2.3, maximum of 13).

In a broad manner, Th, U, Ta and Hf are moderately to weakly negatively correlated with SiO_2, indicating that a heavy-mineral fraction was not strongly accumulated in these sedimentary rocks. On the other hand, the moderate correlation between Zr and Yb (rZr–Yb = +0.50 at $\alpha = 0.5\%$) suggests that the distribution of HREE may be controlled to a certain extent by Zr-rich phases, such as detrital zircon. Possible accumulation of detrital titanate minerals (e.g. rutile, titanite) is further indicated by the moderate correlation between Ta and TiO_2 ($r TiO_2$–Ta = +0.66 at $\alpha = 0.1\%$). It seems however that the distribution of REE was not controlled by that of detrital apatite, as there is no correlation between P_2O_5 and REE ($r P_2O_5$–Yb = +0.03; $r P_2O_5$–La = −0.17).

6. Discussion

6.1. Effects of weathering, heavy-mineral accumulation, diagenesis, and metamorphism on the composition of sedimentary rocks

As will be detailed for each of the following processes, major and trace elements can be subject to important mobilization and fractionation during weathering, mineral accumulation, diagenesis and metamorphism. Hence, in order to properly identify the source characteristics of the studied sedimentary rocks, some control tests must be performed on the geochemical data prior to interpretation.

6.1.1. Weathering in the source area

Weathering involves the conversion of volcanic glass and unstable minerals, mainly feldspars and mica, to clay, as well as oxidization of ferromagnesian components.

Table 2b
Compositions of sedimentary rocks of the Triassic flysch recalculated volatile-free

	Black shale												
	LHA-11	LHA-14	LHA-14	PAZ-03	PAZ-04	PAZ-08	MAS-01	MAS-05	ZIS-02	DAY-01	DAY-02	DAY-03	DZU-03
SiO_2	61.00	69.00	69.03	65.19	66.54	82.56	80.97	73.72	83.76	56.95	76.48	71.92	73.29
TiO_2	1.02	0.73	0.73	0.85	0.86	0.32	0.42	0.60	0.53	0.95	0.54	0.83	0.60
Al_2O_3	24.30	17.65	17.68	18.33	18.35	9.65	10.71	14.28	8.91	24.15	12.75	16.65	10.65
Fe_2O_3	7.19	6.83	6.92	8.76	8.22	3.74	3.60	5.68	3.44	8.12	4.61	5.99	5.77
MnO	0.15	0.05	0.05	0.06	0.07	0.03	0.05	0.05	0.00	0.09	0.04	0.04	0.20
MgO	1.08	1.74	1.75	2.01	1.67	1.18	1.05	1.66	0.58	1.55	1.07	0.50	2.43
CaO	0.16	0.11	0.11	0.17	0.54	0.13	0.35	0.14	0.18	0.06	0.24	0.15	3.62
Na_2O	1.65	1.26	1.24	1.03	1.12	0.24	0.50	0.78	0.87	1.48	2.09	0.88	1.14
K_2O	3.25	2.45	2.29	3.41	2.32	2.06	2.21	2.93	1.54	5.54	1.96	2.77	1.98
P_2O_5	0.06	0.04	0.04	0.05	0.07	<0.026	0.04	0.04	0.07	0.06	0.15	0.13	0.13
LOI	5.24	3.94	3.92	4.84	5.99	2.49	3.14	3.50	3.43	6.49	2.55	5.11	6.69
Total	99.11	98.93	98.04	98.49	99.89	98.61	98.88	98.24	98.20	99.23	99.02	97.27	99.74
Cr	110.80	105.60	104.80	119.90	139.50	54.10	49.20	73.10	63.20	116.90	37.50	62.60	62.50
Sc	19.83	17.10	17.03	18.02	17.82	9.51	11.29	14.04	9.76	19.53	9.13	13.41	9.43
Sr	143.90	480.70	477.90	66.20	215.30	124.50	51.80	34.40	73.20	81.70	49.50	149.80	42.70
V	168.20	139.00	136.20	148.40	149.20	80.60	77.70	124.80	70.80	149.80	54.60	92.80	71.20
Rb	206.11	158.84	142.55	181.32	165.77	121.09	121.74	151.32	82.42	284.97	104.55	141.00	109.51
Y	33.04	15.97	16.42	26.44	32.06	14.58	40.01	23.75	20.27	87.28	27.88	31.08	25.83
Zr	173.25	124.83	122.41	137.66	135.20	95.24	104.65	119.25	125.54	168.06	281.57	234.91	211.42
Nb	27.04	18.72	17.99	20.62	20.59	9.90	12.60	15.75	14.90	23.67	10.81	13.62	13.22
Cs	10.91	5.86	4.48	3.51	7.36	4.12	8.42	5.88	3.93	13.78	4.59	7.11	5.30
La	55.68	33.77	33.33	42.05	45.77	17.38	37.59	33.56	23.45	60.68	26.25	32.73	30.22
Ce	127.41	79.89	78.69	102.11	108.28	38.22	74.57	78.45	55.02	135.69	60.12	73.99	64.76
Pr	13.39	7.92	7.83	9.78	10.86	4.26	9.07	7.81	5.40	15.08	7.04	8.61	7.21
Nd	49.03	28.94	28.74	36.01	40.03	15.86	34.69	28.32	19.60	57.42	27.07	32.87	26.39
Sm	8.90	5.41	5.40	6.71	7.03	2.92	6.24	4.47	3.41	11.37	5.42	6.30	4.93
Eu	1.71	1.15	1.15	1.32	1.31	0.59	0.93	0.76	0.65	2.29	1.10	1.22	0.90
Gd	7.43	4.46	4.35	5.80	5.96	2.60	5.81	3.64	3.01	11.95	5.12	5.03	4.49
Tb	1.01	0.58	0.58	0.79	0.85	0.36	0.91	0.53	0.43	1.98	0.75	0.73	0.69
Dy	5.23	2.90	2.86	4.16	4.59	1.92	5.41	3.17	2.48	11.95	4.08	4.30	3.85
Ho	1.18	0.57	0.57	0.90	1.05	0.43	1.28	0.78	0.61	2.77	0.92	1.02	0.88
Er	3.23	1.32	1.36	2.39	2.73	1.18	3.33	2.16	1.66	7.29	2.46	2.85	2.39
Tm	0.48	0.19	0.19	0.35	0.39	0.17	0.48	0.33	0.24	0.97	0.36	0.42	0.35
Yb	3.34	1.31	1.33	2.37	2.54	1.22	3.00	2.18	1.65	5.88	2.43	2.94	2.40
Lu	0.48	0.21	0.21	0.35	0.37	0.19	0.41	0.31	0.25	0.79	0.35	0.43	0.34
Hf	4.07	2.65	2.67	3.00	2.94	2.04	2.19	2.73	2.74	4.03	5.94	5.29	4.69
Ta	1.85	1.16	1.16	1.29	1.25	0.63	0.75	1.04	0.92	1.68	0.72	0.93	0.97
Th	23.91	15.33	15.68	17.82	16.67	7.62	11.50	13.98	10.22	23.60	10.02	12.21	13.65
U	2.41	1.48	1.48	2.01	2.16	0.95	1.05	1.50	1.40	2.23	2.39	2.94	2.85

Degradation to clay coupled with dissolution reactions induce mobilization and fractionation of many elements in weathering profiles, including rare earth elements (e.g. Morey and Setterholm, 1997). Along with progressive weathering, soils are increasingly depleted in soluble cations such as Ca^{2+} and Sr^{2+} ($\pm Mg^{2+}$), while relatively enriched in insoluble primary minerals like zircon, and Fe, K, Rb, Th and REE, which are strongly partitioned in, or absorbed on, clay minerals, iron oxides and hydroxides (e.g. Nesbitt and Young, 1989). The consequent increase in the Rb/Sr ratio of most rocks during weathering is a good indicator of the degree of weathering. As observed by the low argillization of feldspars, the sandstones have relatively low Rb/Sr ratios ranging from 0.04 to 0.57. By comparison, mafic blocks within the Yamdrock mélange and flysch give average values of 0.04 and 0.15, respectively. As expected, the shales reach much higher Rb/Sr ratios of 0.3–4.8 (with

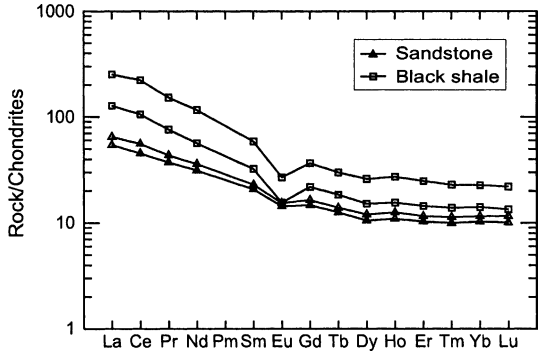

Fig. 5. REE patterns normalized to chondrites for sandstones and black shales from the Mesozoic Yamdrock mélange, in the Beilie and Dazhuqu areas. Normalizing values are from Sun and McDonough (1989).

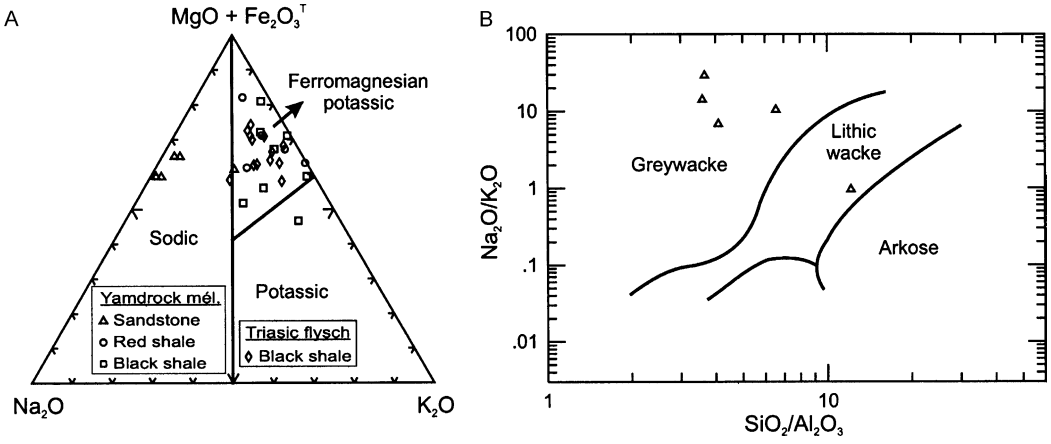

Fig. 6. (A) Classification of sandstones according to Blatt et al. (1980); (B) $\log(Na_2O/K_2O)$ vs. $\log(SiO_2/Al_2O_3)$ discriminating among greywacke, lithic wacke and arkose (after Pettijohn et al., 1973).

an exceptional value of 10.6) and 2.4–7.3 for the black and red shales, respectively.

The Chemical Index of Alteration (CIA) of Nesbitt and Young (1982) quantitatively expresses the degree of weathering of feldspars to clays. The CIA has been established as a general guide of the degree of weathering of source rocks. Using molecular proportions

$$CIA = Al_2O_3/(Al_2O_3 + K_2O + Na_2O + CaO_{Sil}) \times 100,$$

where CaO_{Sil} represents calcium bound in silicate mineral structure. CIA varies from less than 50 for unweathered igneous rocks to near 100 for residual clays; typical shales average about 70–75. Shales of the Yamdrock mélange and flysch have CIA values ranging from 62 to 79, with an average of 72.5 ± 6. Three shales have unrealistic low CIA of 39, 50 and 57. Their CaO content is too high to be structurally enclosed in silicate minerals, which suggests, together with high LOI of 7–14 wt%, that diagenetic or low-T hydrothermal carbonates may be present in a significant amount in these shales. Corrected CIA values of 73, 74 and 70 are obtained by using an average CaO content. Such CIA, in addition with very low CaO/MgO of 0.21 ± 0.11 and fractionation between Rb and Sr (Rb/Sr generally >0.5), suggest that moderate to strong weathering occurred in the source areas of the shales.

The average CIA of the four greywackes is 51.5 ± 3.5, whereas that of the more potassic lithic wacke is 32. However, as observed for the shales, CIA values may also depend on the alteration state of the rock. Hydrothermal alteration tends, in a broad manner, to lower the calculated CIA values of altered greywackes, due mainly to relative CaO (and CO_2) gains and Al_2O_3 losses associated with carbonate alteration (La Flèche and Camiré, 1996). The sampled greywackes do contain small amounts of calcite, with LOI ranging between 2.4 and 5.1 wt%. The very low CIA value of the lithic wacke is due to the relative Al_2O_3 (6.7 wt%) depletion with respect to other elements ($CaO + Na_2O + K_2O = 8.3$ wt%), probably as the result of clays being flushed away by a strong current. Nevertheless, the CIA of greywackes are significantly lower than those of the shales, which suggests, in addition to the slightly higher CaO/MgO of 0.95 ± 0.27 and the lower Rb/Sr values, that they are less weathered. This is to be expected from greywackes, which are considered to have undergone high erosion rates, rapid sedimentation, and therefore a weak to moderate degree of chemical weathering in the source area (La Flèche and Camiré, 1996).

Table 3
Correlation coefficients between major elements and SiO_2 for the sandstones

	Correlation coefficient, r	Student's correlation test, t	Significance level, α (%)
SiO_2–TiO_2	−0.95	−5.40	1
SiO_2–Al_2O_3	−0.97	−7.24	0.5
SiO_2–Fe_2O_3	−0.72	−1.78	10
SiO_2–MnO	−0.81	−2.40	5
SiO_2–MgO	−0.97	−6.71	0.5
SiO_2–CaO	+0.26	+0.46	$\gg 10$
SiO_2–Na_2O	−0.95	−5.14	1
SiO_2–K_2O	+0.62	+1.35	>10
SiO_2–P_2O_5	−0.80	−2.31	10

Table 4
Correlation coefficients between major elements and SiO_2 for the shales

	Correlation coefficient, r	Student's correlation test, t	Significance level, α (%)
SiO_2–TiO_2	−0.55	−3.24	0.5
SiO_2–Al_2O_3	−0.85	−8.05	0.1
SiO_2–Fe_2O_3	−0.65	−4.19	0.1
SiO_2–MnO	−0.19	−0.93	>10
SiO_2–MgO	−0.49	−2.77	1
SiO_2–CaO	−0.36	−1.86	5
SiO_2–Na_2O	−0.28	−1.43	10
SiO_2–K_2O	−0.65	−4.21	0.1
SiO_2–P_2O_5	−0.13	−0.65	$\gg 10$

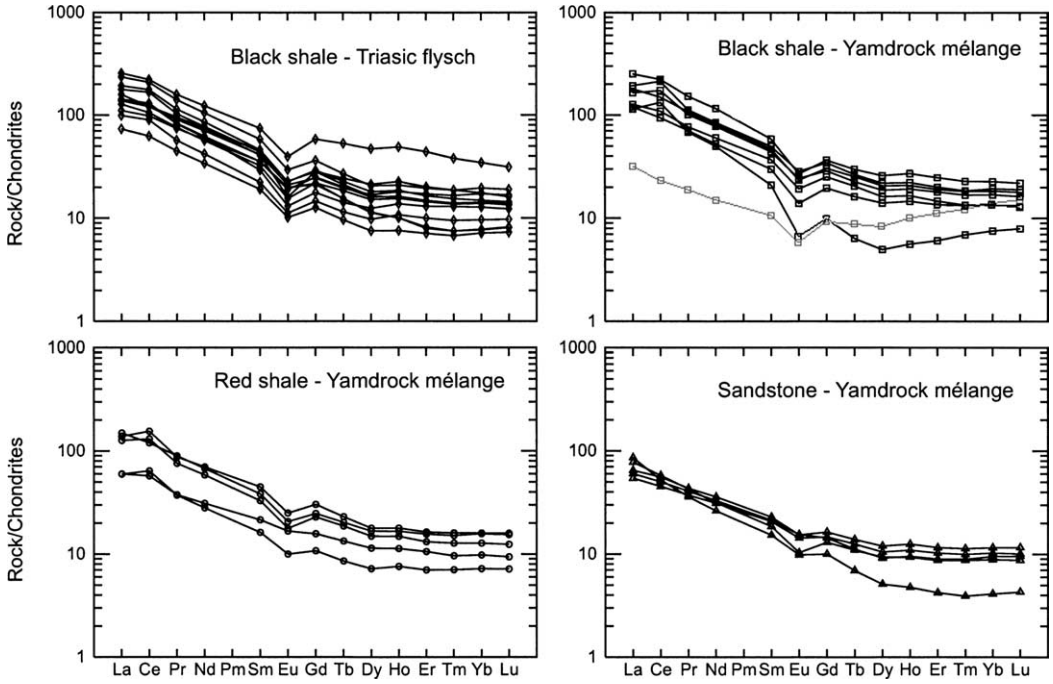

Fig. 7. REE patterns normalized to chondrite for sedimentary rocks from the Mesozoic Yamdrock mélange and the Triassic flysch. Normalizing values are from Sun and McDonough (1989).

6.1.2. Sedimentary sorting and heavy-mineral accumulation

Heavy-mineral accumulation during sedimentary sorting can considerably complicate interpretations of sediment provenance by producing irregular chemical variations in some trace elements (McLennan et al., 1993). For instance, Zr and Hf may be concentrated in the coarser fraction of the sediment due to zircon accumulation in the latter. In the same manner, REE and Th abundances may depend on accumulation of monazite, apatite, zircon or titanite (e.g. Crichton and Condie, 1993). Although the moderate correlation observed between the pairs Zr–Yb and Ti–Ta suggests some accumulation of zircon and titanite, it appears, nevertheless, that heavy-mineral accumulation did not have a significant effect on the whole-rock geochemical signature of the Neo-Tethyan sediments, as only weak and not systematic covariations are observed between LREE and Th (Fig. 9A), HREE and Hf (Fig. 9B), and Ta/La and Ti (Fig. 9C). Accumulation of apatite and allanite is counter-indicated by the weak fractionation of La/Sm, Tb/Yb and Ta/La ratios (Fig. 9). Accumulation of monazite is further counter-indicated by an average $(Gd/Yb)_N$ ratio of 1.7 ± 0.4, typical of post-Archean sediments and most upper crustal igneous rocks (even small amounts of monazite result in significant increases in the $(Gd/Yb)_N$ ratio; McLennan, 1989; McLennan and Taylor, 1991). Although some samples tend to align along the accumulation trends of zircon and titanite (Fig. 9A and B), accumulation of these heavy minerals is probably not significant since the Ta/La ratio is not really fractionated (Fig. 9C).

The effect of heavy-mineral accumulation and hydraulic sorting on the geochemical signature of a sediment can also be evaluated by comparing the relative abundances of insoluble elements, such as Al_2O_3 and TiO_2, which are generally unaffected by weathering processes and which are preferentially incorporated in clay particles of argillaceous beds, and Zr and Hf, commonly partitioned in coarser grained zircon of sandy beds. This is schematized in the $(Hf \times 36.2)$–$(Al_2O_3 \times 15)$–$(TiO_2 \times 300)$ triangular diagram of Garcia et al. (1994), where close grouping of Neo-Tethyan sedimentary rocks away from the Hf pole indicates that Hf abundances were not controlled by zircon accumulation and that the rocks are fairly juvenile (Fig. 10). Finally, on a graph of Th/Sc vs. Zr/Sc (Fig. 9D), the sandstones and shales fall on the trend defined by active margin turbidites, a trend consistent with igneous chemical differentiation, i.e. provenance, being the primary control (McLennan et al., 1993). Our sedimentary rocks show high Th/Sc and Zr/Sc ratios similar to those of passive margin turbidites, but do not show a substantial increase in Zr/Sc with respect to Th/Sc indicative of ziron enrichment. These results confirm that the Neo-Tethyan sandstones and shales are passive margin sediments derived from highly chemically differentiated igneous rocks, but not affected by significant sedimentary recycling such as zircon accumulation. Intermediate SiO_2/Al_2O_3 ratios further suggest absence of significant sedimentary reworking (McLennan et al., 1993).

6.1.3. Diagenesis and metamorphism

Significant albitization, illitization, feldspar dissolution, as well as carbonate, quartz and limonite diagenetic cementation, accompanied by important chemical changes, are well documented in some reservoir sandstones

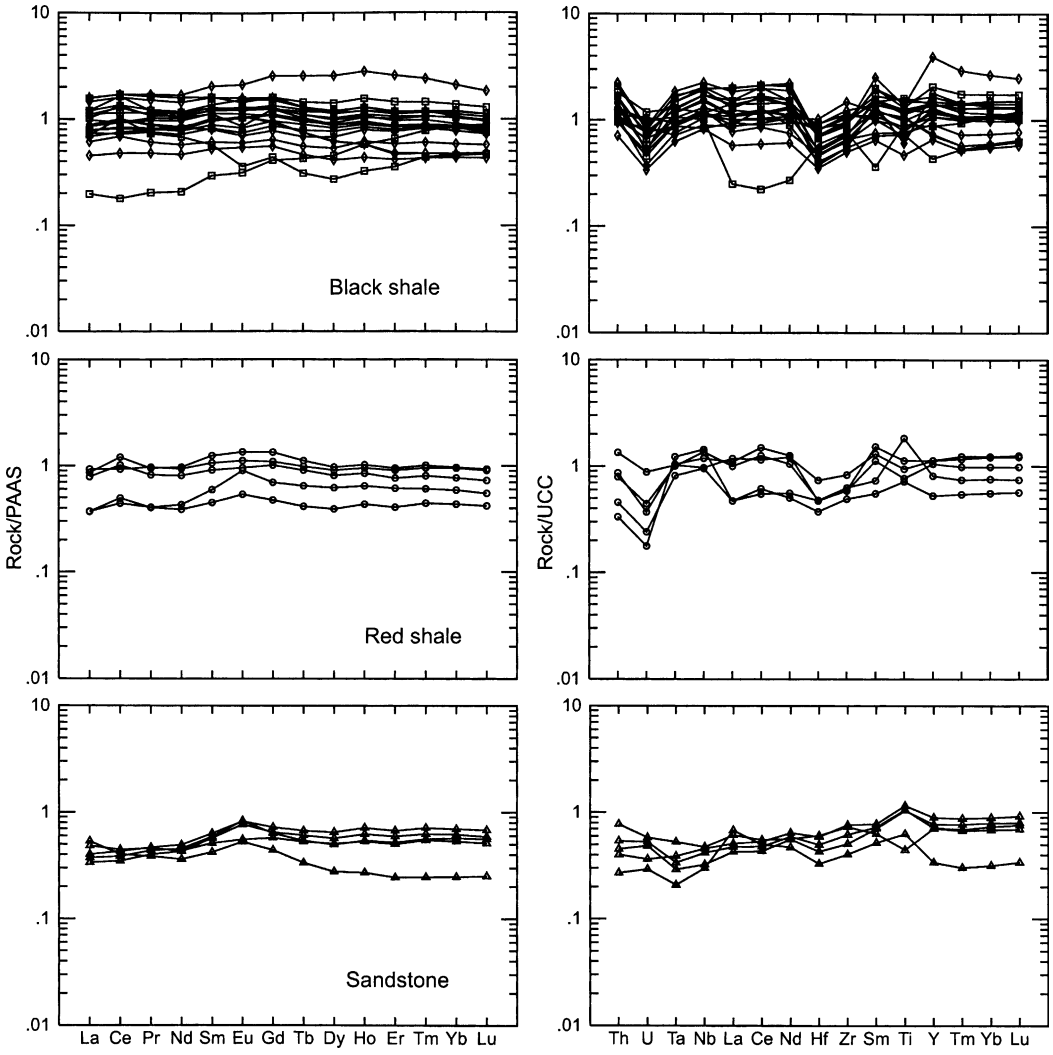

Fig. 8. REE patterns normalized to Post-Archean average Australian shale (PAAS) (left column) and multi-element patterns normalized to the average upper continental crust (UCC) (right column) for sedimentary rocks from the Mesozoic Yamdrock mélange and the Triassic flysch. Normalizing values are from Taylor and McLennan (1985), except Nb, Ta and Ti that are from McLennan (2001).

(e.g. Land et al., 1987). Albitization of feldspars may explain why the greywackes have low K_2O/Na_2O ratios. However, in finer grained siliciclastic sediments, the concentrations of most major components are not significantly changed during diagenesis (Wintsch and Kvale, 1994). Among the many reactions occurring during diagenesis, only illitization of smectite and dissolution of calcite appear to have significant effects (K_2O gains and CaO losses, respectively) on the bulk composition of mudstones (La Flèche and Camiré, 1996). Other elements like REE, Hf, Ta, Th, Zr, Cr, Co and Sc are transported in the terrigenous components or carried largely as suspended rather than dissolved loads during erosion, transfer, transport and sedimentation, because they are relatively insoluble in most natural waters. They may be massively transferred from source to sediment, and therefore used as reliable provenance indicators (Taylor and McLennan, 1985). Diagenetic and metamorphic reactions (up to upper amphibolite grade) appear to redistribute these elements among various diagenetic and metamorphic minerals without significant remobilization of the elements into or out of the system (Ohr et al., 1991; Bau, 1991; Totten and Blatt, 1993). Accordingly, neither diagenesis nor metamorphism (up to partial melting reactions) appear to significantly affect bulk-rock REE and multi-element patterns. Geodynamic interpretations made from such trace-element patterns are therefore more significant and reliable than those obtained from major element compositions.

6.2. Geodynamic interpretation

The parameters that are known and should be taken into consideration before further chemical constraints can be placed on the provenance of sedimentary rocks south of the YZSZ are as follows: (1) The Yamdrock mélange and flysch units contain blocks of mafic rocks; (2) A geochemically

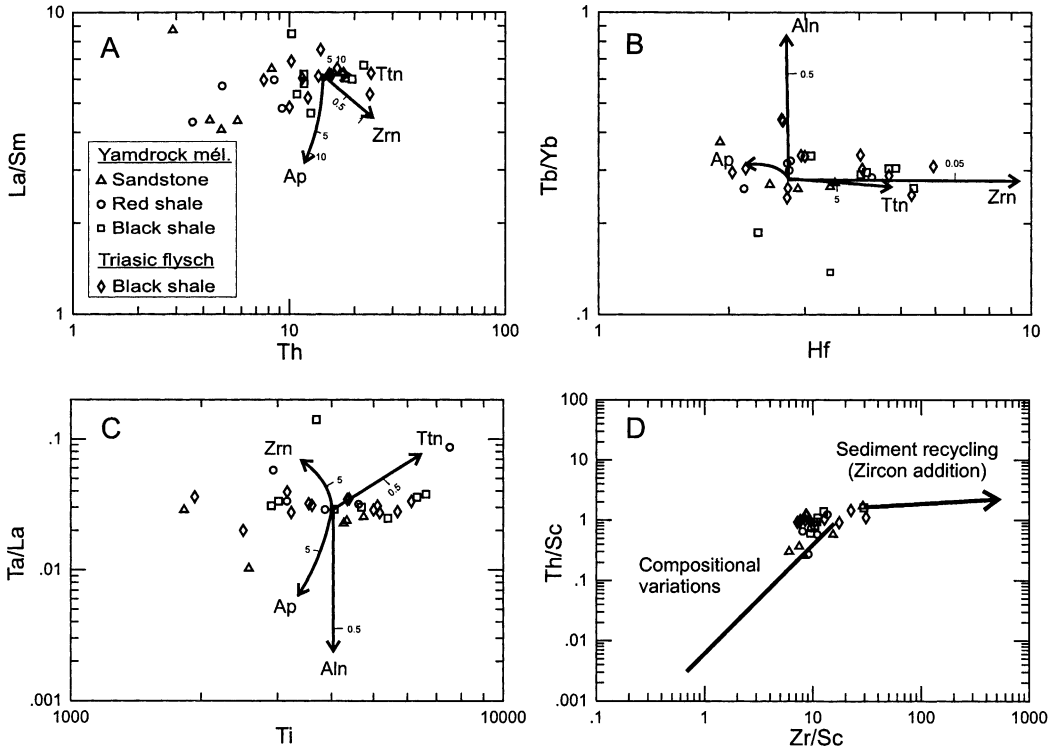

Fig. 9. Calculated accumulation trends of detrital apatite (Ap), allanite (Aln), titanite (Ttn) and zircon (Zrn) showing the effects of heavy-mineral accumulation on selected trace elements and trace element ratios (from La Flèche and Camiré, 1996). (A) La/Sm vs. Th; (B) Tb/Yb vs. Hf; (C) Ta/La vs. Ti. (D) Plot of Th/Sc vs. Zr/Sc showing enrichment of zircon as opposed to compositional variations of the provenance; trends of compositional variations and sediment recycling from McLennan et al. (1993).

highly differentiated (calc-alkaline) granitic block was also found in the Triassic flysch; (3) Limited sedimentary reworking and low Hf/TiO_2 and Hf/Al_2O_3 (Fig. 10) indicate that the sandstones and shales are moderately immature and most likely monocyclic; (4) Moderate to strong chemical weathering of the source areas suggests, nevertheless, that the sediments were not simply unconsolidated debris eroded from active volcanoes, but probably derive from a continental passive margin.

On the basis of whole-rock chemistry, sedimentary rocks of the Yamdrock mélange and flysch mostly have an old upper continental crustal (OUC) provenance, according to the terrane classification of McLennan et al. (1993). The rocks, especially the shales, generally have evolved major element compositions (e.g. moderately high CIA, SiO_2/Al_2O_3, K_2O/Na_2O), which reflect a dominance of upper crustal granitic sources and a relatively severe weathering history. The rocks also have substantial negative Eu anomalies (average Eu/Eu* of 0.6 ± 0.1 and 0.8 ± 0.04 for the shales and greywackes, respectively), which reflect intracrustal geochemical differentiation involving considerable separation of plagioclase (Taylor and McLennan, 1985). Enrichment of incompatible over compatible elements, such as LREE enrichment (Fig. 7) and high Th/Sc ratios (Fig. 9D), reflects felsic component provenance compositions, whereas high Rb/Sr (>0.5) and Th/U (>3.8) reflect weathering. The different REE pattern of one individual black shale (smaller LREE enrichment) corresponds more to the young differentiated arc (YDA) terrane type of McLennan et al. (1993). The YDA provenance component represents young (mantle-derived) volcanic and plutonic igneous rocks of island and continental arcs that were affected by intracrustal differentiation, such that they possess significant negative Eu anomalies (Eu/Eu* of 0.6 in

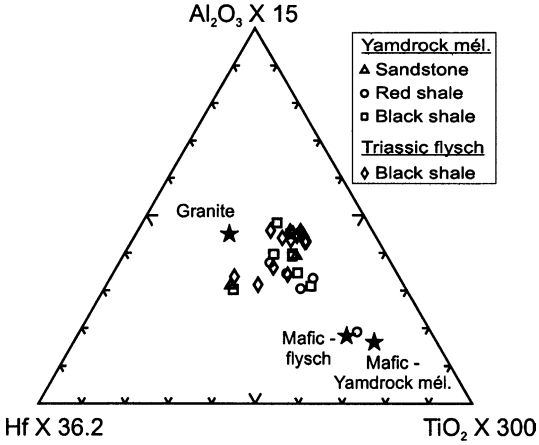

Fig. 10. $(Hf\times36.2)$–$(Al_2O_3\times15)$–$(TiO_2\times300)$ triangular diagram of Garcia et al. (1994) modified by La Flèche and Camiré (1996). Increasing maturity of sedimentary rocks is indicated by the arrow. The filled stars indicate the average composition of mafic blocks and one granitic block in the sedimentary units (Dupuis et al., 2003a,b, 2004).

this case). However, the shale was significantly affected by weathering processes, a feature not expected for a YDA provenance. As a matter of fact, the shale has a low, but not abnormal, CIA of 65 and a fairly high Rb/Sr of 4.8. A mixture of young undifferentiated arc (YUA) and OUC, such as observed in mature arc environments (McLennan et al., 1990), is probably a more realistic provenance. Moreover, apart from the REE pattern, chemical compositions and ratios of this individual shale are very similar to those of our total turbiditic shale population.

The high Th/U ratios observed in the Yamdrock mélange and flysch sedimentary rocks could also indicate the contribution of granulitic felsic gneisses, i.e. the contribution of deeply eroded cratonic areas. However, low Rb/Cs ratios (average of 25 ± 10) suggest that such a contribution was not significant (La Flèche and Camiré, 1996). Low Y/Ni ratios (<1) rather indicate the contribution of a mafic to ultramafic component to the Neo-Tethyan turbidites. Low Cr/Ti (<0.04) and Cr/V (<1.2) ratios further reflect the probable absence within the turbidites of chromite and ultramafic components characteristic of the ophiolitic sequences lying north of the flysch and Yamdrock mélange sequences. The contrasting geochemistry of mafic blocks within the sedimentary units and the overlying ophiolitic units have already shown that these distinct geological units also come from different tectonic environments (Dupuis et al., 2003, 2004).

Examples of sedimentary rocks dominated by OUC include abundant cratonic shales, most passive margin turbidites and foreland basin sediments derived from the older exposed continental crust (McLennan et al., 1993). For the Yamdrock mélange and flsych sedimentary rocks, flat REE patterns averaging 1, when normalized to average Post-Archean Australian Shale (PAAS) and upper continental crust (UCC; Fig. 8), are typical of sedimentary rocks derived from a passive margin. By using the Hf-Al_2O_3–TiO_2 ternary diagram (Fig. 10), we can see that the sedimentary rocks may be obtained from mixing of detrital material derived from mafic and felsic rocks of the Indian passive margin, onto which the flysch and Yamdrock mélange units have been deposited. In fact, LREE of the Neo-Tethyan turbiditic sedimentary rocks are strongly fractionated with $(La/Sm)_N$ ratios falling in between those of the mafic rocks and the granitic value (Fig. 11). Low $(Ta/Th)_N$ ratios further indicate that genesis of the igneous source involved subduction and (or) crustal recycling processes (Fig. 11A). This signature is most probably derived from a granitic component similar to the granitic block of the flysch, which has a very evolved geochemical signature, and because the mafic rocks rather have an intraplate geochemical signature (Dupuis et al., 2003, 2004).

Th/Sc and Hf/Sc ratios are especially sensitive to fluctuations in mafic vs. felsic sources, Sc being preferentially concentrated in the former, while Th and Hf in the latter (La Flèche and Camiré, 1996). Sedimentary rocks of the Yamdrock mélange and flysch have Th/Sc and Hf/Sc

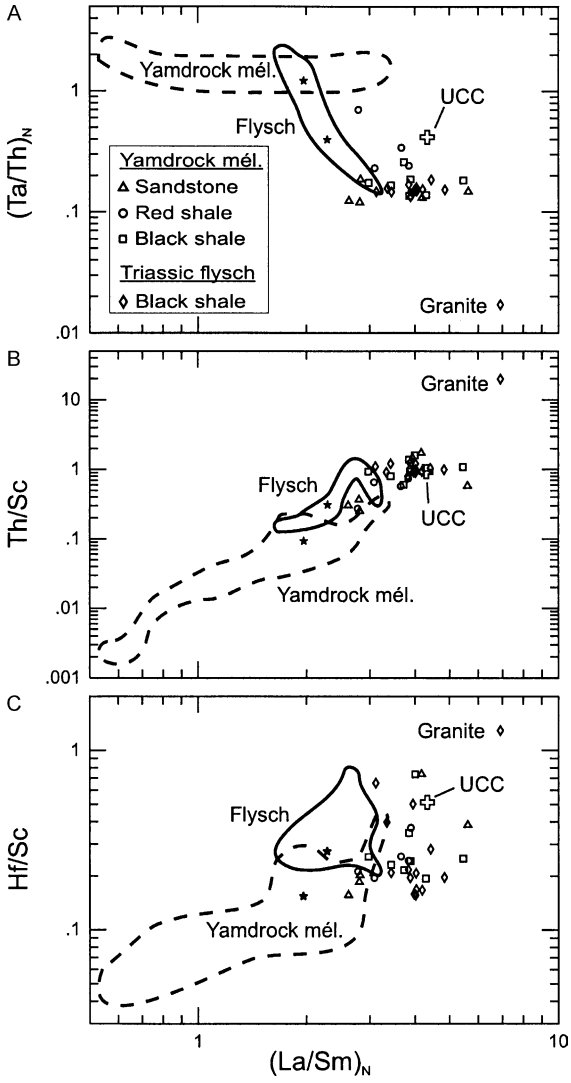

Fig. 11. $(Ta/Th)_N$ (A), Th/Sc (B) and Hf/Sc (C) vs. $(La/Sm)_N$. Chondrite normalizing (N) values from Sun and McDonough (1989). Fields represents mafic blocks found in the sedimentary units with average values represented by the black stars; the field representing mafic blocks from the ophiolitic mélange would fall past the most distant end of the Yamdrock mélange field (Dupuis et al., 2003a,b, 2004). Upper continental crust (UCC) values from Taylor and McLennan (1985), Ta and Sc from McLennan (2001).

ratios closer to those of the average mafic rocks than the granitic one, especially for Hf, indicating that the contribution of mafic intraplate components in the source was probably more important than that of granitic components (Fig. 11B and C). However, we have to keep in mind that the chemistry of mafic rocks from the Triassic flysch has itself been partly overprinted by partial crustal assimilation of the Indian Plate associated with magmatism resulting from opening of the Neo-Tethys basin (Dupuis et al., 2003, 2004). While the upper continental crust is usually believed to have a granodiorite composition, slight positive Ti anomalies (when normalized to UCC) are reminiscent of enriched mafic blocks of intraplate affinity found in the sedimentary units.

Based solely on their geochemistry, sedimentary rocks of the Triassic flysch and Yamdrock mélange thus seem both to have been deposited on a continental passive margin setting, and to be derived from a similar OUC source. However, based on other geological observations, the Triassic flysch and Mesozoic Yamdrock mélange are representative of distinct specific geodynamic settings (Fig. 12). Our results confirm that the Triassic flysch is composed of turbidite sequences deposited on the Indian passive margin and extending on the growing Neo-Tethys basin, as previously illustrated by Nicolas (1989) (Fig. 12A). The flysch is the result of erosion of igneous and sedimentary rocks of the Indian upper continental crust (UCC). Contemporaneously with initial rifting, mafic dykes were produced by partial melting of the lower continental crust (LCC) by an continental intraplate alkaline magma source below the Indian Plate (Dupuis et al., 2003, 2004). Together with remnants of Cambrian granite batholiths (Yin and Harrison, 2000), they were eroded and incorporated within the flysch unit.

As mentioned in the geological setting description, during the opening of the Neo-Tethys basin in the Late Triassic–Early Jurassic, compression caused by the Indian Block approaching from the south resulted in the initiation of a north-dipping intra-oceanic subduction zone, active from at least Late Jurassic to the end of Early Cretaceous times (Girardeau et al., 1984; Göpel et al., 1984; Miller et al., 2003; Zyabrev et al., 1999; Ziabrev et al., 2003).

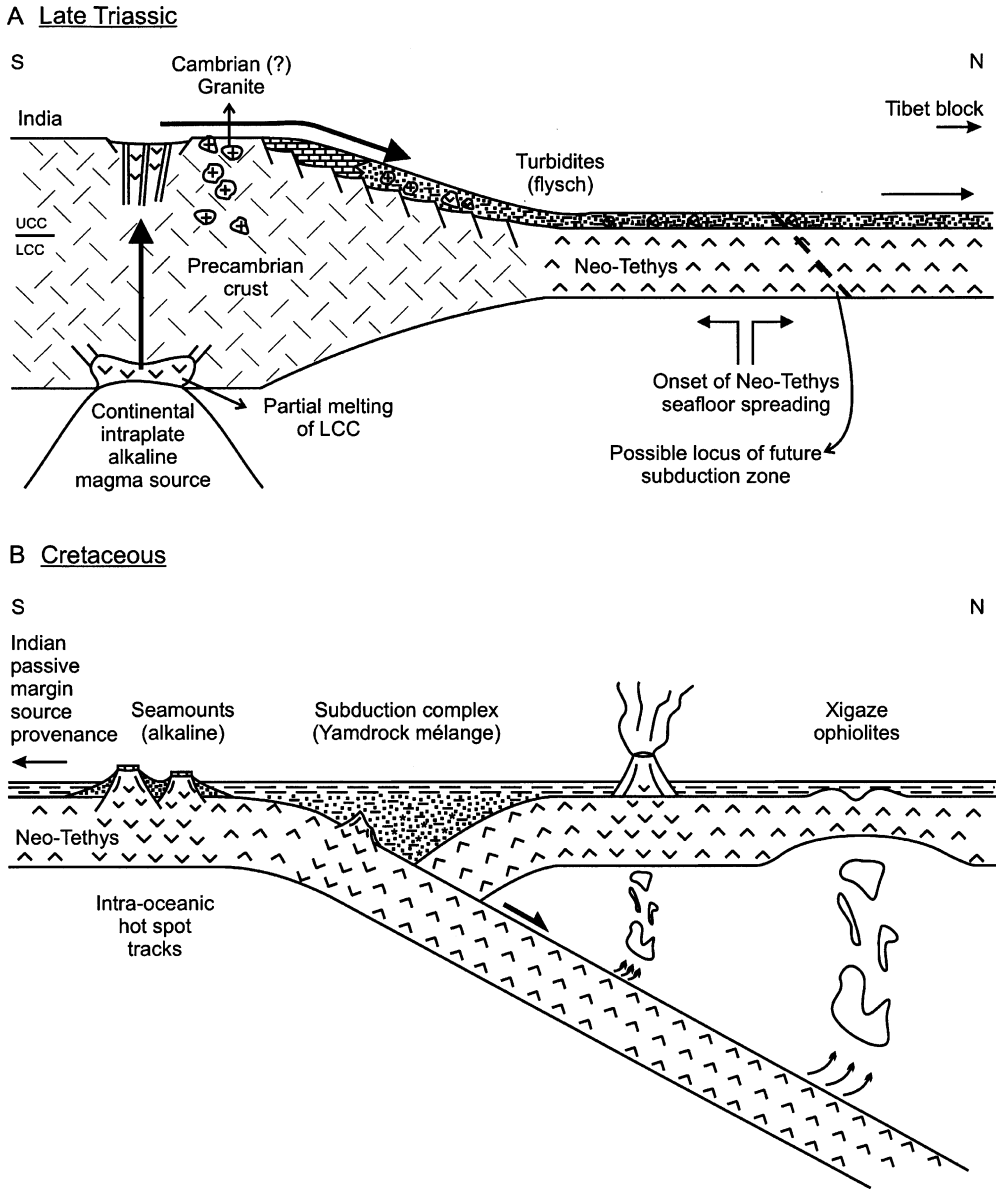

Fig. 12. (A) Late Triassic geodynamic situation at the time of flysch deposition; (B) Cretaceous geodynamic situation at the time of intra-oceanic subduction and Yamdrock mélange deposition. Not to scale. The geodynamic setting of the ophiolites is greatly simplified and is shown solely to illustrate the initial spatial distribution between the now adjacent units. UCC: upper continental crust, LCC: lower continental crust.

Structural and tectonostratigraphic features of the Yamdrock mélange recall its formation within an intra-oceanic subduction complex (Mercier et al., 1984; Searle et al., 1987; Aitchison et al., 2000), and the unit has been interpreted to consist mostly of material off-scraped from the down-going Tethyan slab (Chang, 1984; Ziabrev et al., 2001) (Fig. 12B). Our results indicate that this material represents Indian continental passive margin deposits, including deeper-water radiolarites that were transported on the growing Neo-Tethys ocean floor. According to paleomagnetic (Pozzi et al., 1984; Abrajevitch, 2002) and tomographic (Van der Voo et al., 1999) investigations, the subduction zone that generated the Xigaze ophiolites and the Yamdrock mélange subduction complex was located at equatorial to low northern latitudes at least 1000–1500 km south of the southern margin of Asia and about 2000 km north of the northern margin of India. The turbidite deposits would thus have travelled some 2000 km to the north on the growing Neo-Tethys ocean floor, a scenario observed in modern ocean basins. Moreover, the Yamdrock mélange contains remnants of alkaline seamounts (e.g. Mercier et al., 1984; Searle et al., 1987; Liu and Einsele, 1999; Aitchison et al., 2000) of intra-oceanic intraplate geochemical affinity (Dupuis et al., 2003, 2004). These alkaline seamounts were thus probably derived from the same intraplate alkaline magma source that generated the mafic dykes, now as blocks within the Triassic flysch, and which evolved from continental to oceanic after the rifting event. Albanian and Greek ophiolitic sequences of the Mesozoic Tethys ocean are also thrust over a sub-ophiolitic mélange, which has similar geological characteristics to the Yamdrock mélange (Bortolotti et al., 2004). The origin of both mélanges is probably a multi-stage process, with sedimentary (turbidite deposition) and tectonic (off-scraping and progressive obduction) events.

6.2.1. Implications for Himalayan geology

Several isotopic studies have been conducted on rocks of the Himalayan Series, including the YZSZ (e.g. compilation by Najman et al., 2000), but few trace element data are available for sedimentary rocks of the same area. Nevertheless, we were able to correlate our geochemical data with clastic metasedimentary rocks of greywacke composition from the Garhwal Himalaya (Ahmad et al., 2000). As discussed previously, plots of immobile-element ratios can discriminate between clastic units derived from contrasting source regions, and such plots remain robust during high-grade metamorphism. Using such immobile-element ratios (Fig. 13), sandstones and shales from the Yamdrock mélange and Triassic flysch correlate especially well with metasedimentary rocks from the High Himalayan (HH) Crystalline Series and Outer Lesser Himalayan (OLH) Series. Except for the Munsiari and Ramgarh Groups (field labelled ILH on Fig. 13A), which have developed metamorphism up to garnet grade (Ahmad et al., 2000), there is also a good correlation with some metasedimentary rocks from the Inner Lesser Himalayan Series, rocks that fall in the 'HH +O∠H' field on Fig. 13A. Usually, a linear array in the Zr/Al_2O_3–TiO_2/Zr space (Fig. 13B) is defined by sediments of variable size fractions derived from the same source area; the array is caused by the differences in hydraulic behavior between minerals containing Zr and those containing Al_2O_3–TiO_2 (Fralick and Kronberg, 1997). The main differences observed for our rocks, i.e. displacement towards the Sc pole (Fig. 13A) and towards higher TiO_2/Zr ratios (Fig. 13B), may be attributed to the mafic contribution detected in the geochemistry of the studied rocks.

Sedimentary rocks of the Yamdrock mélange and the Triassic flysch also correlate well with shales and sandstones of the Cretaceous Tianba flysch (Fig. 13),

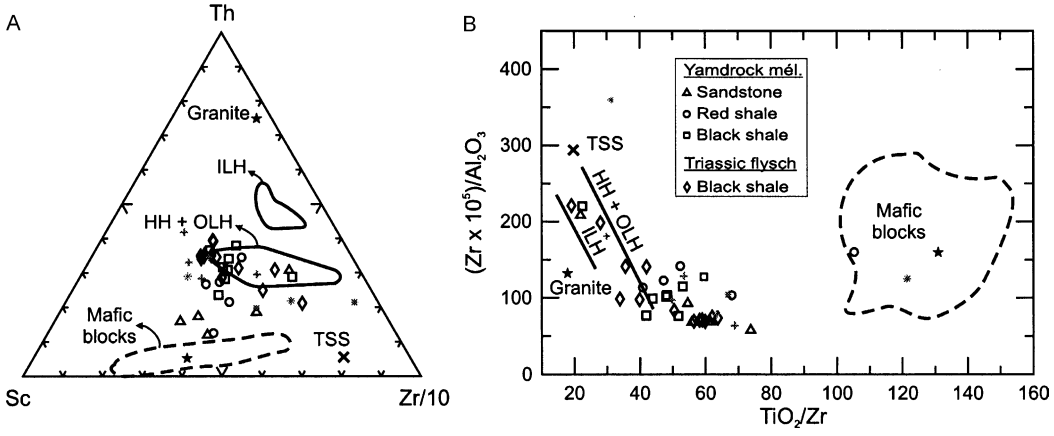

Fig. 13. (A) Th–Sc–Zr ternary plot for sandstones and shales of the Yamdrock mélange and Triassic flysch (after Bhatia and Crook, 1986); (B) $(Zr'10^5)/Al_2O_3$ ratio diagram for the same data set (after Fralick and Kronberg, 1997). Grey crosses and asterisks represent shales and sandstones, respectively, of the Tianba flysch, southern Tibet (Zhu, 2003). Clastic metasedimentary rocks of greywacke composition from Garhwal Himalaya (Ahmad et al., 2000) are shown for comparison. TSS, Tethyan Sedimentary Series; HH, Higher Himalaya crystalline series; ILH and OLH, Inner and Outer Lesser Himalaya Series, respectively (field labelled ILH on (A) includes only the Munsiari and Ramgarh Groups of the ILH Series). Dashed fields represent mafic blocs from the Yamdrock mélange with average value represented by the star (Dupuis et al., 2003a,b, 2004).

located to the south of the YZSZ, i.e. just southeast of our study area (Zhu, 2003). In agreement with detrital zircon analyses, paleocurrent data and paleontological data (Myrow et al., 2003), the uniformity in sedimentary rocks from the Mesozoic Yamdrock mélange, the Triassic flysch, and the Cretaceous Tianba flysch, which altogether cover a large spatial area and a large time span, as well as the good correlation with distinct lithotectonic units of the Himalaya, all tend to support the 'continuous margin' model. According to this model, all three main lithotectonic zones, the Greater, Lesser and Tethyan Himalaya, represent different proximal-to-distal parts of the ancient passive margin of northern India (Brookfield, 1993; Searle, 1986; Corfield and Searle, 2000). It appears that element and isotope geochemistry give complementary information about the tectonic setting, source and depositional history of sedimentary rocks, and that conclusions must not be drawn on limited data.

7. Conclusion

The geochemical signature of sandstones, red shales and black shales of the Yamdrock mélange and flysch units lying immediately south of the YZSZ, in southern Tibet, do not present significant variations between the different rock types and geological units, and are concordant with a continental passive margin source. Shales have CIA (average of 72.5 ± 6) typical of shales around the world, which suggests, in addition with important fractionation between Rb and Sr, that moderate to strong weathering occurred in their source areas. Greywackes have undergone higher erosion rates, rapid sedimentation, and therefore weak to moderate chemical weathering (average CIA of 51.5 ± 3.5). Despite this fairly important chemical weathering, the whole-rock chemical signature of both sandstones and shales was not affected by significant sedimentary recycling nor heavy-mineral accumulation. REE patterns indicate that the Neo-Tethyan turbidites generally derive from a mostly felsic old upper continental crust (UCC) source. Slight positive Ti anomalies, with respect to the UCC, in addition with characteristic element ratios, indicate a mafic contribution to the source. This mafic contribution most probably comes from mafic blocks of enriched intraplate geochemical affinity found in the sedimentary units. Thus, the sedimentary rocks outcropping south of the YZSZ were derived from the old Indian continental crust, including remnants of granite batholiths and intraplate mafic blocks. Turbidites of the Triassic flysch were deposited on the Indian passive margin, whereas turbidites and radiolarites of the Yamdrock mélange were deposited on the growing Neo-Tethys ocean floor and incorporated in a subduction complex mélange. The results of this study are in agreement with the formation of all Himalayan lithotectonic units along a continuous passive margin of Northern India.

Acknowledgements

We would like to thank the funding organization (NSERC/Grant no. 1253 to R.H.) for financial support of the Tibet project. The first author also thanks the NSERC (scholarship PGS B) and FQRNT for financial support. We are also thankful to M. Choquette for microprobe analyses and to R. Gosselin for ICP-AES and ICP-MS analyses. We are grateful to Marc Richer La Flèche for fruitful discussion during preparation of an early version of the manuscript. The manuscript has further benefited from critical comments by A.J. Barber, A. Yin, J.C. Aitchison, K. Condie, and Y. Najman.

References

Abrajevitch, A., 2002. Paleomagnetism of the Dazhuqu Terrane. Yarlung Zangbo Suture Zone, Southern Tibet. M.Phil. Thesis, University of Hong Kong.

Ahmad, T., Harris, N., Bickle, M., Chapman, H., Bunbury, J., Prince, C., 2000. Isotopic constraints on the structural relationships between the Lesser Himalayan Series and the High Himalayan Crystalline Series, Garhwal Himalaya. Geological Society of America Bulletin 112, 467–477.

Aitchison, J.C., Badengzhu, Davis, A.M., Liu, J., Luo, H., Malpas, J., McDermid, I., Wu, H., Ziabrev, S., Zhou, M.F., 2000. Remnants of a Cretaceous intra-oceanic subduction system within the Yarlung-Zangbo suture (southern Tibet). Earth and Planetary Science Letters 183, 231–244.

Aitchison, J.C., Davis, A.M., Abrajevitch, A.V., Ali, J.R., Badengzhu, Liu, J., Luo, H., McDermid, I., Ziabrev, S., 2003. Stratigraphic and sedimentological constraints on the age and tectonic evolution of the Neo-Tethyan ophiolites along the Yarlung Tsangpo suture zone, Tibet. In: Dylek, Y., Robinson, P.T. (Eds.), Ophiolites in Earth History Special Publications 218. Geological Society, London, pp. 147–164.

Allègre, C.J., Coutillot, V., Tapponnier, P., et al., 1984. (32) Structure and evolution of the Himalaya–Tibet orogenic belt. Nature 307, 17–22.

Bau, M., 1991. Rare-earth element mobility during hydrothermal and metamorphic fluid-rock interactions and the significance of the oxidation state of Eu. Chemical Geology 93, 219–230.

Beck, R.A., Burbank, D.W., Sercombe, W.J., Riley, G.W., Barndt, J.K., 1995. Stratigraphic evidence for an early collision between northwest India and Asia. Nature 373, 55–58.

Bhatia, M.R., Crook, K.A.W., 1986. Trace element characteristics of graywackes and tectonic setting discrimination of sedimentary basin. Contributions to Mineralogy and Petrology 92, 181–193.

Blatt, H., Middleton, G.V., Murray, R.C., 1980. Origin of Sedimentary Rocks. Prentice-Hall, Englewood Cliffs, NJ.

Bortolotti, V., Chiari, M., Marucci, M., Marroni, M., Pandolfi, L., Principi, G., Saccani, E., 2004. Comparison among the Albanian and Greek ophiolites. In search of constraints for the evolution of the Mesozoic Tethyan ocean. Ofioliti 29, 19–35.

Brookfield, M.E., 1993. The Himalayan passive margin from Precambrian to Cretaceous times. Sedimentary Geology 84, 1–35.

Burg, J.P., Chen, G.M., 1984. Tectonics and structural zonation of southern Tibet, China. Nature 311, 219–223.

Burg, J.P., Leyreloup, A., Girardeau, J., Chen, G.M., 1987. Structure and metamorphism of a tectonically thickened continental crust; the Yalu

Zangbo suture zone (Tibet). Philosophical Transactions of the Royal Society of London A 321, 67–86.

Chang, C., 1980. Les caractéristiques tectoniques et l'évolution de la zone de suture du Yarlung-Zangbo. In: Mercier, J.L., Li, G.C. (Eds.), Mission Franco-Chinoise au Tibet: Étude Géologique et Géophysique de la Croûte Terrestre et du Manteau Supérieur du Tibet et de L'Himalaya. Éditions du Centre National de la Recherche Scientifique, Paris, France, pp. 341–350.

Corfield, R.I., Searle, M.P., 2000. Crustal shortening estimates across the north Indian continental margin, Ladakh, NW India. In: Khan, M.A., Treloar, P.J., Searle, M.P., Jan, M.Q. (Eds.), Tectonics of the Nanga Parbat Syntaxis and the Western Himalaya Geological Society of London Special Publication 170, pp. 395–410.

Crichton, J.G., Condie, K.C., 1993. Trace elements as source indicators in cratonic sediments: a case study from the Early Proterozoic Libby Creek Group, southeastern Wyoming. Journal of Geology 101, 319–332.

DeCelles, P.G., Gehrels, G.E., Quade, J., LaReau, B., Spurlin, M., 2000. Tectonic implications of U–Pb zircon ages of the Himalayan orogenic belt in Nepal. Science 288, 497–499.

Dubois-Côté, V., 2004. Pétrologie et géochimie des ophiolites de la Zone de Suture du Yarlung Zangbo (ZSYZ), Tibet: Implications géodynamiques. M.Sc. Thesis, Université Laval, 231p.

Dubois-Côté, V., Hébert, R., Wang, C.S., Li, Y.L., Dostal, J., 2003. Petrology and geochemistry of Yarlung Zangbo Suture Zone (YZSZ) ophiolites, Tibet: Geodynamic implications. GAC-MAC-SEG Joint Annual Meeting Abstracts (Vancouver) 28, 188.

Dupuis, C., Hébert, R., Huot, F., Wang, C.S., Li, Y.L., Li, Z.J., 2003. Petrology and geochemistry of Tethysian Jurassic and Triassic provinces related to the Yarlung Zangbo Suture Zone (YZSZ), Tibet. In: 18th Himalaya–Karakorum–Tibet Workshop Abstracts, pp. 38–40.

Dupuis, C., Hébert, R., Wang, C.S., Li, Y.L., Li, Z.J., 2004. Petrology and geochemistry of Tethyan mélange and flysch units adjacent to the Yarlung Zangbo Suture Zone (YZSZ), Southern Tibet. AOS Transactions AGU 85, Joint Assembly Supplements, Abstract V43A-06.

Fralick, P.W., Kronberg, B.I., 1997. Geochemical discrimination of clastic sedimentary sources. Sedimentary Geology 113, 111–124.

France-Lanord, C., Derry, L., Michard, A., 1993. Evolution of the Himalaya since Miocene time: isotopic and sedimentological evidence from the Bengal Fan. In: Treloar, P.J., Searle, M.P. (Eds.), Himalayan Tectonics Geological Society of London Special Publication 7, pp. 603–621.

Gaetani, M., Garzanti, E., 1991. Multicyclic history of the northern India continental margin (northwestern Himalaya). American Association of Petroleum Geologist Bulletin 75, 1427–1446.

Galy, A., France-Lanord, C., Derry, L., 1996. The Late Oligocene–Early Miocene Himalayan belt constraints deduced from isotopic compositions of Early Miocene turbidites in the Bengal Fan. Tectonophysics 260, 109–118.

Gansser, A., 1974. The ophiolitic mélange, a world-wide problem on Tethyan examples. Eclogae Geologicae Helvetiae 67, 479–507.

Gansser, A., 1980. The significance of the Himalayan suture zone. Tectonophysics 62, 37–53.

Garcia, D., Fonteilles, M., Moutte, J., 1994. Sedimentary fractionation between Al, Ti, and Zr and the genesis of strongly peraluminous granites. Journal of Geology 102, 411–422.

Girardeau, J., Marcoux, J., Zao, Y., 1984. Lithologic and tectonic environment of the Xigaze ophiolite (Yarlung Zangbo suture zone, Southern Tibet, China): kinematics of its emplacement. Eclogae Geologicae Helvetiae 77, 153–170.

Göpel, C., Allègre, C.J., Xu, R.-H., 1984. Lead isotopic study of the Xigaze ophiolite (Tibet): the problem of the relationship between magmatites (gabbros, dolerites, lavas) and tectonites (harzburgites). Earth and Planetary Science Letters 69, 301–310.

Guilmette, C., Hébert, R., 2003. Occurrence of high-grade metabasites in the Buma and Bainang ophiolitic mélanges along the Yarlung Tsangpo Suture Zone, South Tibet: a dismembered dynamothermal sole? In: 18th Himalaya–Karakorum–Tibet Workshop Abstracts, pp. 54–55.

Harrison, T.M., Yin, A., Grove, M., Lovera, O.M., 1921. The Zedong window: a record of superposed Tertiary convergence in southeastern Tibet. Journal of Geophysical Research 105, 1–19230.

Hébert, R., Varfalvy, V., Huot, F., Wang, C.S., Liu, Z.F., 2000. Yarlung Zangbo ophiolites, southern Tibet revisited. In: 15th Himalaya–Karakorum–Tibet Workshop Abstracts, Earth Science Frontiers, 7, pp. 124–126.

Hébert, R., Wang, C.S., Varfalvy, V., Huot, F., Beaudoin, G., Dostal, J., 2001. Yarlung Zangbo Suture Ophiolites and their suprasubduction zone setting. In: 16th Himalaya–Karakorum–Tibet Workshop Abstracts. Journal of Asian Earth Sciences, 19, 27–28.

Hébert, R., Huot, F., Wang, C.S., Liu, Z.F., 2003. Yarlung Zangbo ophiolites (Southern Tibet) revisited: Geodynamic implications from the mineral record. In: Dylek, Y., Robinson, P.T. (Eds.), Ophiolites in Earth History. Geological Society, London. Special Publication, pp. 165–190.

Hodges, K.V., 2000. Tectonics of the Himalaya and southern Tibet from two perspectives. Geological Society of America Bulletin 112, 324–350.

Huot, F., Hébert, R., Varfalvy, V., Beaudoin, G., Wang, C.S., Liu, Z.F., Cotten, J., Dostal, J., 2002. The Beimarang mélange (southern Tibet) brings additional constraints in assessing the origin, metamorphic evolution and obduction processes of the Yarlung Zangbo ophiolite. Journal of Asian Earth Sciences 21, 307–322.

Huyghe, P., Galy, A., Mugnier, J.L., France-Lanord, C., 2001. Propagation of the thrust system and erosion in the Lesser Himalaya: geochemical and sedimentological evidence. Geology 29, 1007–1010.

Jaeger, J.-J., Courtillot, V., Tapponnier, P., 1989. Paleontological view of the ages of the Deccan Traps, the Cretaceous/Tertiary boundary and the India–Asia collision. Geology 17, 316–319.

Klootwijk, C.T., Gee, J.S., Peirce, H.W., Smith, G.M., McFadden, P.L., 1992. An early India–Asia contact: paleomagnetic constraints from Ninetyeast Ridge, ODP Leg 121. Geology 20, 395–398.

Klootwijk, C.T., Conaghan, P.J., Nazirullah, R., de Jong, K.A., 1994. Further paleomagnetic data from Chitral (Eastern Hindukush): evidence for an early India–Asia contact. Tectonophysics 237, 1–25.

La Flèche, M.R., Camiré, G., 1996. Geochemistry and provenance of metasedimentary rocks from the Archean Golden Pond sequence (Casa Berardi mining district, Abitibi sub province). Canadian Journal of Earth Sciences 33, 676–690.

La Flèche, M.R., Camiré, G., Jenner, G.A., 1998. Geochemistry of post-Acadian, Carboniferous continental intraplate basalts from the Maritimes Basin, Magdalen Islands, Québec, Canada. Chemical Geology 148, 115–136.

Land, S.L., Milliken, K.L., McBride, E.F., 1987. Diagenetic evolution of Cenozoic sandstones, Gulf of Mexico sedimentary basin. Sedimentary Geology 50, 195–225.

Lee, T.Y., Lawver, L.A., 1995. Cenozoic plate reconstruction of Southeast Asia. Tectonophysics 251, 85–138.

Le Fort, P., 1996. Evolution of the Himalaya. In: Yin, A., Harrison, T.M. (Eds.), The Tectonic Evolution of Asia. Cambridge University Press, New York, pp. 95–106.

Lin, B., 1984. Les strates du Permien inférieur et la faune coralienne dans la région centre-sud du Tibet. In: Mercier, J.L., Li, G.C. (Eds.), Mission Franco-Chinoise au Tibet: Étude Géologique et Géophysique de la Croûte Terrestre et du Manteau Supérieur du Tibet et de L'Himalaya. Éditions du Centre National de la Recherche Scientifique, Paris, France, pp. 77–107.

Liu, G., Einsele, G., 1996. Various types of olistostromes in a closing ocean basin, Tethyan Himalaya (Cretaceous, Tibet). Sedimentary Geology 104, 203–226.

Liu, G., Einsele, G., 1999. Jurassic sedimentary facies and paleogeography of the former Indian passive margin in southern Tibet. Geological Society of America Special Paper 328, 75–108.

Mahéo, G., Bertrand, H., Guillot, S., Villa, I.M., Keller, F., Capiez, P., 2004. The South Ladakh ophiolites (NW Himalaya, India): an

intra-oceanic theoleiitic arc origin with implication for the closure of the Neo-Tethys. Chemical Geology 203, 273–303.

Matsuoka, A., Kobayashi, K., Takei, M., Nagahashi, Yang, Q.T., Wang, Y., Takei, M., Zeng, Q.G., 2001. Early Middle Jurassic (Aalenian) radiolarian fauna from the Xialu chert in the Yarlung Zangbo Suture Zone, southern Tibet. In: Metcalfe, I., Smith, J.M.B., Morwood, M., Davidson, I. (Eds.), Faunal and Floral Migrations and Evolution in SE Asia–Australia. Balkema, Rotterdam, pp. 105–110.

Matsuoka, A., Yang, Q., Kobayashi, K., Takei, M., Nagahashi, T., Zeng, Q., Wang, Y., 2002. Jurassic–Cretaceous radiolarian biostratigraphy and sedimentary environments of the Ceno-Tethys: records from the Xialu Chert in the Yarlung-Zangbo Suture Zone, southern Tibet. Journal of Asian Earth Sciences 20, 277–287.

Matte, P., Mattauer, M., Olivet, J.M., Griot, D.A., 1997. Continental subduction beneath Tibet and the Himalayan orogen: a review. Terra Nova 9, 264–270.

McLennan, S.M., 1989. Rare earth elements in sedimentary rocks: influence of provenance and sedimentary processes. Mineralogical Society of America, Review in Mineralogy 21, 169–200.

McLennan, S.M., 2001. Relationships between the trace element composition of sedimentary rocks and upper continental crust. Geochemistry, Geophysics, Geosystems 2. $G^3$2, paper 2000GC000109.

McLennan, S.M., Taylor, S.R., 1991. Sedimentary rocks and crustal evolution: tectonic settings and secular trends. Journal of Geology 99, 1–21.

McLennan, S.M., Taylor, S.R., McCulloch, M.T., Maynard, J.B., 1990. Geochemical and Nd–Sr isotopic compositions of deep-sea turbidites: crustal evolution and plate tectonic association. Geochimica Cosmochimica Acta 54, 2015–2050.

McLennan, S.M., Hemming, S., McDaniel, D.K., Hanson, G.N., 1993. Geochemical approaches to sedimentation, provenance, and tectonics. Geological Society of America Special Paper 284, 21–40.

Mercier, J.L., et al., 1984. (29) la collision Inde-Asie côté Tibet. In: Mercier, J.L., Li, G.C. (Eds.), Mission Franco-chinoise au Tibet 1980: Étude Géologique et Géophysique de la Croûte Terrestre et du Manteau Supérieur du Tibet et de L'Himalaya. Éditions du Centre National de la Recherche Scientifique, Paris, France, pp. 341–350.

Miller, C., Thoeni, M., Frank, W., Schuster, R., Melcher, F., Meisel, T., Zanetti, A., 2003. Geochemistry and tectonomagmatic affinity of the Yungbwa Ophiolite, SW Tibet. Lithos 66, 155–172.

Molnar, P., Tapponnier, P., 1975. Cenozoic tectonics of Asia: effects of a continental collision. Science 189, 419–426.

Morey, G.B., Setterholm, D.R., 1997. Rare earth elements in weathering profiles and sediments of Minnesota; implications for provenance studies. Journal of Sedimentary Research 67, 105–115.

Myrow, P.M., Hughes, N.C., Paulsen, T.S., Williams, I.S., Parcha, S.K., Thompson, K.R., Bowring, S.A., Peng, S.C., Ahluwalia, A.D., 2003. Integrated tectonostratigraphic analysis of the Himalaya and implications for its tectonic reconstruction. Earth and Planetary Science Letters 212, 433–441.

Najman, Y., Bickle, M., Chapman, H., 2000. Early Himalayan exhumation: isotopic constraints from the Indian foreland basin. Terra Nova 12, 28–34.

Nesbitt, H.W., Young, G.M., 1982. Early Proterozoic climates and plate motions inferred from major element chemistry of lutites. Nature 299, 715–717.

Nesbitt, H.W., Young, G.M., 1989. Formation and diagenesis of weathering profiles. Journal of Geology 97, 129–147.

Nicolas, A., 1989. Structures of Ophiolites and Dynamic of Oceanic Lithosphere. Kluwer, Dordrecht. 368 p.

Ohr, M., Halliday, A.N., Peacor, D.R., 1991. Sr and Nd isotopic evidence for punctuated clay diagenesis, Texas Gulf Coast. Earth and Planetary Science Letters 105, 110–126.

Patriat, P., Achache, J., 1984. India–Eurasia collision chronology has implications for crustal shortening and driving mechanism of plates. Nature 311, 615–621.

Pettijohn, F.J., Potter, P.E., Siever, R., 1973. Sand and Sandstone. Springer, New York.

Pini, G.A., 1999. Tectonosomes and olistostromes in the argille scagliose of the Northern Apennines, Italy. Geological Society of America Special Paper 335, 70.

Pozzi, J.P., Westphal, M., Girardeau, J., Besse, J., Zhou, Y.X., Chen, X.Y., Xing, L.S., 1984. Paleomagnetism of the Xigaze ophiolite and flysch (Yarlung Zangbo suture zone, southern Tibet): latitude and direction of spreading. Earth and Planetary Science Letters 70, 383–394.

Ratschbacher, L., Frisch, W., Liu, G., Chen, C., 1981. Distributed deformation in southern and western Tibet during and after India–Asia collision. Journal of Geophysical Research 99, 19817–19945.

Robinson, D.M., DeCelles, P.G., Patchett, P.J., Garzione, C.N., 2001. The kinematic evolution of the Nepalese Himalaya interpreted from Nd isotopes. Earth and Planetary Science Letters 192, 507–521.

Rowley, D.B., 1996. Age of initiation of collision between India and Asia: a review of stratigraphic data. Earth and Planetary Science Letters 145, 1–13.

Searle, M.P., 1986. Structural evolution and sequence of thrusting in the Himalayan, Tibetan-Tethys and Indus suture zones of Zanskar and Ladakh, Western Himalaya. Journal of Structural Geology 8, 923–936.

Searle, M.P., Windley, B.F., Coward, M.P., Cooper, D.J.W., Rex, A.J., Rex, D., Li, T.D., Xiao, X.C., Jan, M.Q., Thakur, V.C., Kumar, S., 1987. The closing of Tethys and the tectonics of the Himalaya. Geological Society of America Bulletin 98, 678–701.

Shackleton, R.M., 1981. Structure of southern Tibet: Report on a traverse from Lhasa to Khatmandu organized by Academia Sinica. Journal of Structural Geology 3, 97–105.

Sun, S.S., McDonough, W.F., 1989. Chemical and isotopic systematics of oceanic basalts: implications for mantle composition and processes. Geological Society of London Special Publication 42, 313–345.

Tapponnier, P., Mercier, J.L., Proust, F., et al., 1981a. (27) The Tibetan side of the India–Eurasia collision. Nature 294, 405–410.

Tapponnier, P., Mercier, J.L., Armijo, R., Han, T., Zhou, J., 1981b. Field evidence for an active normal faulting in Tibet. Nature 294, 410–414.

Taylor, S.R., McLennan, S.M., 1985. The Continental Crust: Its Composition and Evolution. An Examination of the Geological Record Preserved in Sedimentary Rocks. Blackwell, Oxford.

Totten, M.W., Blatt, H., 1993. Alterations in the non-clay-mineral fraction of pelitic rocks across the diagenetic low-grade metamorphic transition, Ouachita Mountains, Oklahoma and Arkansas. Journal of Sedimentary Petrology 63, 899–908.

Van der Voo, R., Spakman, W., Bijwaard, H., 1999. Tethyan subducted slab under India. Earth and Planetary Science Letters 171, 7–20.

Wang, C.S., Liu, Z., Hébert, R., 2000. The Yarlung-Zangbo paleo-ophiolite, southern Tibet: implications for the dynamic evolution of the Yarlung-Zangbo Suture Zone. Journal of Asian Earth Sciences 18, 651–661.

Wang, X.B., Xiao, X.C., Cao, Y.G., Zheng, H.X., 1984. Geological map of the ophiolite zone along the middle Yarlung Zangbo River, Xizang (Tibet), Second Geological and Geophysical brigade of geological Bureau of the Tibet Autonomous Region. Publishing House of Surveying and Mapping, Beijing, P.R. China.

Wintsch, R.P., Kvale, C.M., 1994. Differential mobility of elements in burial diagenesis of siliciclastic rocks. Journal of Sedimentary Petrology 64, 349–361.

Wu, H.R., 1993. Upper Jurassic and Lower Cretaceous radiolarians of Xialu chert, Yarlung Zangbo ophiolite belt, southern Tibet. In: Blueford, J.R., Murchey, B.L. (Eds.), Radiolaria of Giant and Subgiant Fields of Asia, Nazarov Memorial Volume Micropaleontological Special Paper 6, pp. 115–136.

Yin, A., Harrison, T.M., 2000. Geologic evolution of the Himalayan–Tibetan orogen. Annual Review in Earth and Planetary Sciences 28, 211–280.

Yin, A., Harrison, T.M., Ryerson, F.J., Wenji, C., Kidd, W.S.F., Copeland, P., 1994. Tertiary structural evolution of the Gangdese thrust system, southeastern Tibet. Journal of Geophysical Research 99, 18175–18201.

Zhu, B., 2003. Sedimentology, petrography, and tectonic significance of Cretaceous to Lower Tertiary deposits in the Tingri-Gyangtse area, southern Tibet. Ph.D. Thesis, State University of New York at Albany, 213p.

Ziabrev, S.V., Aitchison, J.C., Badengzhu, Davis, A.M., Luo, H., Liu, J.B., McDermid, I., Malpas, J., 2000. Oceanic deposits in the Yarlung-Tsangpo suture zone: Structural setting, radiolarian ages and their tectonic implications. In: 15th Himalaya–Karakorum–Tibet Workshop Abstracts, Earth Science Frontiers, 7, 118.

Ziabrev, S.V., Aitchison, J.C., Badengzhu, Davis, A.M., Luo, H., Liu, J.B., 2001. More about the missing Tethys: Bainang terrane Tibet. In: 16th Himalaya–Karakorum–Tibet Workshop Abstracts. Journal of Asian Earth Sciences 19, 82–83.

Ziabrev, S.V., Aitchison, J.C., Abrajevitch, A.V., Badengzhu, Davis, A.M., Luo, H., 2003. Precise radiolarian age constraints on the timing of ophiolite generation and sedimentation in the Dazuqu terrane, Yarlung-Tsangpo suture zone, Tibet. Journal of the Geological Society of London 160, 591–599.

Ziabrev, S.V., Aitchison, J.C., Abrajevitch, A.V., Badengzhu, Davis, A.M., Luo, H., 2004. Bainang Terrane, Yarlung-Tsangpo suture, southern Tibet (Xizang, China): a record of intra-Neotethyan subduction-accretion processes preserved on the roof of the world. Journal of the Geological Society of London 161, 1–17.

Zyabrev, S.V., Aitchison, J.C., Badengzhu, Davis, A.M., Luo, H., Malpas, J., 1999. Radiolarian biostratigraphy of supra-ophiolite sequences in the Xigaze area, Yarlung Tsangpo suture, Southern Tibet (preliminary report). Radiolaria 17, 13–19.

Zyabrev, S.V., Aitchison, J.C., Badengzhu, Davis, A.M., Luo, H., Liu, J.B., 2000. Tethyan relics in the Yarlung-Tsangpo suture, Tibet: structural setting, radiolarian ages and their tectonic significance. Ninth Meeting of the International Association of Radiolarian Paleontologists INTERRAD 2000 Program with Abstracts 2000; 72.